Contents lists available at http://qu.edu.iq

Al-Qadisiyah Journal for Engineering Sciences

Journal homepage: https://qjes.qu.edu.iq

Structural behavior of concentrically loaded GFRP-RPC circular columns

Mohamed Qassim Kadhim* *and Hassan Falah Hassan*

Department of Civil Engineering, College of Engineering, Mustansiriyah University, Baghdad, Iraq

ARTICLE INFO

Article history:
Received 00 December 0000
Received in revised form 00 January 0000
Accepted 00 February 0000

Keywords:
Concrete column
Glass fiber reinforced polymer
Hoops
Reactive powder concrete
Spirals

ABSTRACT

The behavior of reinforced concrete (RC) members with glass fiber reinforced polymer (GFRP) bars has been the focus of several studies in previous years. However, a study to investigate the behavior of reactive powder concrete (RPC) columns reinforced with GFRP bars (GFRP-RPC) has not been conducted. This study aimed to study the structural behavior of circular columns fully reinforced with GFRP bars and hoops or spirals. In the present study, the behavior of GFRP-RPC circular columns under axial load is studied with the effect of four variables: longitudinal reinforcement ratio, transverse reinforcement ratio, transverse reinforcement configuration (hoops vs. spirals), and type of longitudinal reinforcement (GFRP, steel, and hybrid). Twenty circular columns with a diameter of 150 mm and a height of 1000 mm were cast and tested, divided into seven groups. Results discuss failure modes, axial load capacity, deformations (displacement and strains), and ductility. Test results indicate that the load capacity of the columns increased by ranging from approximately 46 to 56.25% when the longitudinal reinforcement ratio increased from 1.77 to 3.55%, also increased the transverse reinforcement ratio from 1.24 to 2.48% enhanced the load capacity ranging from approximately 5.13 to 19.1%. Moreover, the nominal capacity of GFRP-RPC columns was compared with the design equations so, the results were verified.

1. Introduction

Reinforced concrete (RC) columns carry vertical loads from the top to bottom floors to the base. The potential failure of columns poses a significant risk, potentially resulting in catastrophic construction incidents [1]. Circular RC columns are used as piles and bridge piers because they are easy to make, strong, and attractive in all directions under seismic and wind stresses [2]. Conventional RC's reinforcing steel corrodes in coastal areas, severe climates, or corrosion-prone surroundings. Steel is prohibited in MRI rooms and radiation facilities. Fiber-reinforced polymer (FRP) materials are an excellent choice due to their noncorrosive, nonconductive, and nonmagnetic properties [1]. The use of FRP as an alternative to steel in RC structures has become increasingly popular [3]. Among various types of FRPs, glass FRP (GFRP) bars are commonly employed in the construction industry, primarily because of their lower cost [3]. GFRP bars have become more affordable due to a broader market and more competition. GFRP bars reinforce parking garages, concrete bridges, water tanks, and tunnels [4]. GFRPs' promising mechanical and chemical qualities have drawn interest, so, civil engineers prefer RC with GFRP bars for infrastructure [5,6]. Several studies on FRP bars have enhanced international standards and design guidelines. For example, in CAN/CSA S806-12 [7], the role of FRP bars in compression for both flexural and

* *Corresponding author.*
E-mail address: *mohammedkasim9244@gmail.com* (Mohamed Qassim Kadhim)

https://doi.org/10.30772/qjes.2024.145922.1079

compression members' capacities was neglected. However, in CSA S807-19 [8], their contribution is now recognized and considered as part of these members' overall capacity. Similar to ACI 440.1R-06 [9], ACI 440.1R-15 [3] did not recommend using FRP bars as the longitudinal reinforcement in concrete compression members. GFRP bars were recently approved in compression members under ACI 440-22 [10] standards; however, their contribution to compression members' maximum load capacity was ignored. GFRP bars behave differently under compressive loads because their compression strength is much lower than their tensile strength. GFRP bars and RPC together can be used because the ACI 440.1R-15 guide [3] states, "The greater the compressive strength of concrete, the better it will be until the effect of FRP bar appears, where compatibility occurs between the two materials that have high strength." In the early 1990s, RPC, a cementitious composite, was invented in France. The first RPC bridge, Canada's Sherbrook Bridge, was built in July 1997. RPC exhibits exceptional mechanical and physical characteristics, including ultra-high strength and excellent ductility. This unique form of concrete achieves maximum density through precise particle gradients in the mix, thereby enhancing its microstructure. That is done by utilizing fine components with pozzolanic qualities, such as silica fume, and adjusting the chemical properties of Portland cement to foster the formation of the strongest hydrates [11]. The axial compression testing revealed that steel and RPC could effectively collaborate initially. The ultimate failure mode of the column was described as a splitting failure occurring at the column's end, accompanied by a longitudinal crack extending toward the middle [12]. In another study, three transverse reinforcement diameters 4, 6, and 8 mm were employed with spacing distances of 100, 140, and 175 mm. The significance of the transverse reinforcement diameter outweighed that of the spacings between transverse reinforcement in the standard concrete short column. The most substantial enhancement in the ultimate capacity, resulting from diameter changes, reached 203%, while changes in spacing yielded a 179% increase [13]. The axial compressive strength of the steel-reinforced RPC column was improved by the longitudinal reinforcement ratio, steel shape ratio, and transverse stirrup ratio. The post-peak strength is increased by increasing the stirrup ratio [14]. Solid circular GFRP-RC columns subjected to concentric loading have been tested to assess their load capacity, ductility, confinement efficiency, and superiority compared to steel-reinforced columns. Under concentric axial compression, GFRP-reinforced high-strength concrete (HSC) columns and steel columns exhibit similar performance. GFRP bar-reinforced HSC columns showed superior support for axial loads before the increase in load eccentricity. The replacement of steel reinforcement with an equivalent amount of GFRP reinforcement in HSC specimens that were subjected to concentric axial load resulted in a 30% reduction in ductility. Nevertheless, the closely spaced spirals contributed to enhanced ductility and post-peak load-displacement behavior in HSC specimens reinforced with GFRP bars [15]. Increasing the reinforcement ratio from 0.36% to 3.24% enhanced the load capacity of GFRP-RC specimens from 3.4% to 25.7% and raised the average peak strain at peak load from 2.64% to 75.6%, compared to plain concrete specimens. The contribution of GFRP bars ranged from 0.72% to 6.71% at the peak load capacity of GFRP-RC specimens [16]. GFRP-reinforced columns exhibited behavior similar to that of steel-reinforced columns. Despite this similarity, they demonstrated a lower nominal capacity. The increased GFRP's longitudinal reinforcement ratio has led to an increase in the columns' nominal capacity. The increase of longitudinal reinforcement in GFRP-RC columns increases the load capacity (P_n). The nominal capacities (P_n) of GFRP-RC columns were 6.7% lower than those of steel-RC columns, although their maximum capacities (P_{max}) were comparable [17]. Transversely reinforced GFRP specimens demonstrated 15% higher ductility and 12.3% lower capacity than steel reinforcement. Adding longitudinal reinforcing bars and decreasing the GFRP spiral pitch would increase the member's load capacity and ductility. Transverse reinforcement lessens the load capacity gap between steel and GFRP-reinforced columns [18]. For hollow concrete columns (HCCs) reinforced with GFRP bars and spirals, increasing the reinforcement ratio from 1.89 to 3.79% had no significant effect on the peak load (only increased by 5 to 10%), but significantly enhanced the confinement efficiency from 1.43 to 2.23 and the ductility factor from 1.36 to 3.05 for the HCCs reinforced with GFRP bars and spirals. The GFRP longitudinal reinforcement contributed to resisting the peak loads by an average of 11% of the ultimate capacity. The HCCs reinforced with GRFP bars performed better than their solid counterparts [19].

2. Research significance

From the previous studies, it can be noticed that there is a significant amount of investigation on the strength of ordinary concrete columns reinforced with steel or FRP bars. However, with RPC being a relatively new material to the industry, no data exists on FRP-RPC columns. The behavior of GFRP-RPC circular columns under axial load is studied with the effect of four variables in the current study. These are the longitudinal reinforcement ratio, transverse reinforcement ratio, transverse reinforcement configuration (hoops vs. spirals), and type of longitudinal reinforcement (GFRP, Steel, and Hybrid).

3. Experimental program

3.1. Concrete

RPC used in this study contains a high content of Portland cement as the primary cementitious material, besides silica fume as a second supplementary cementitious component. Both the sand-cement ratio (s/c) and the water-cement ratio (w/c) are low. The superplasticizer has been used in an appropriate proportion to give flowable concrete. Moreover, a superplasticizer is used, known commercially as Viscocrete-171 precast produced by Sika company. Mixing ratios according to the study of Hassan [20] used to get maximum compressive strength and flow of 95% according to ASTM C109 [21] and ASTM C1437 [22], where this study depended on previous research [9, 23]. The RPC with cement can be treated as isotopic or transverse isotropic material and there are different techniques available [24-25]. The RPC mix was used in the present research to cast all columns and control specimens, as listed in Table 1. By testing concrete cylinders in compression following ASTM C39 [26], it was possible to determine the concrete's compressive strength. The specimens exhibited an average compressive strength of 85 MPa. Additionally, a splitting tensile test, following ASTM C496 [27], was conducted to obtain the tensile strength of the concrete. The specimens exhibited an average splitting tensile strength of 7.75 MPa.

3.2 GFRP bars

The GFRP producer Nanjing Fenghui Composite Co. Ltd. [28] evaluated the GFRP bars in accordance with ASTM D7205 [29]. No. 3 high-modulus (HM) GFRP bars (CAN/CSA S807-19 [8]) with a nominal diameter of 10 mm (Fig. 1) were used to reinforce the circular column specimens in the longitudinal direction. No. 2 HM GFRP circular hoops and spirals with a

nominal diameter of 6 mm (Fig. 2 and Fig. 3) were used to reinforce the corresponding columns transversely.

Table 1. Properties of the RPC mix.

Cement K_g/m^3	Sand K_g/m^3	Silica fume* %	Silica fume K_g/m^3	w/c	*Viscocrete 171 precast %
900	990	25	225	0.18	5

* Percent of cement weight

The transverse reinforcement had an outer diameter of 120 mm. The hoops had an overlap length of 60 mm. The GFRP reinforcement was produced through the pultrusion process, wherein E-glass fibers were impregnated with a high-durability resin. Additionally, the reinforcement featured a sand-coated surface, augmenting the bond and facilitating force transfer between the bars and the concrete. The mechanical properties of the reinforcement as reported by the manufacturer are provided in Table 2.

Figure 1. GFRP longitudinal reinforcement used in this study.

Figure 2. GFRP hoops used in this study.

Table 2. Mechanical properties of GFRP reinforcement *.

Type No.	Bar size	Nominal Diameter (mm)	Ultimate tensile strength (MPa)	Modulus of Elasticity (GPa)	Weight (g/m)	Transverse shear strength (MPa)
B100-6	#2	6	896	46	77.4	150
B100-10	#3	10	827	46	159	

* As provided by the manufacturer.

3.2. Steel reinforcement

In this study, deformed steel reinforcement of 10 mm diameter was employed for longitudinal bars in both Steel and Hybrid columns. The mechanical properties of Grade 60 steel bars utilized in this study are shown in Table 3. The bar test results (ϕ10 mm) satisfy ASTM A615-5a [30] requirements.

Figure 3. GFRP spirals used in this study.

Table 3. Steel reinforcing properties.

Properties	Analysis	Limits of specification requirement ASTM-A615-5a [30]
Nominal Diameter (mm)	10	-
Yield stress, f_y (MPa)	466.33	≥ 420
Ultimate stress, f_u (MPa)	626.33	≥ 550
Elongation %	9.3	9 % min

3.3. Specimen's details

Twenty circular columns were tested under concentric axial compression load. Eighteen were fully reinforced with GFRP bars and hoops or spirals, and two reference columns were reinforced with longitudinal steel bars and hybrid bars (three steel bars and three GFRP bars). Specimens were 150mm in diameter and 1000mm tall with a 15mm concrete cover. The dimensions, reinforcement scheme, and configuration of the tested specimens are shown in Fig. 4. The test matrix was arranged to evaluate the influences of longitudinal reinforcement ratios, transverse reinforcement ratios, transverse reinforcement configuration (hoops vs. spirals), and type of longitudinal reinforcement (GFRP, Steel, and Hybrid). The test matrix and reinforcement details of the column specimens are summarized in Table 4. Each specimen is identified with a two-part code.

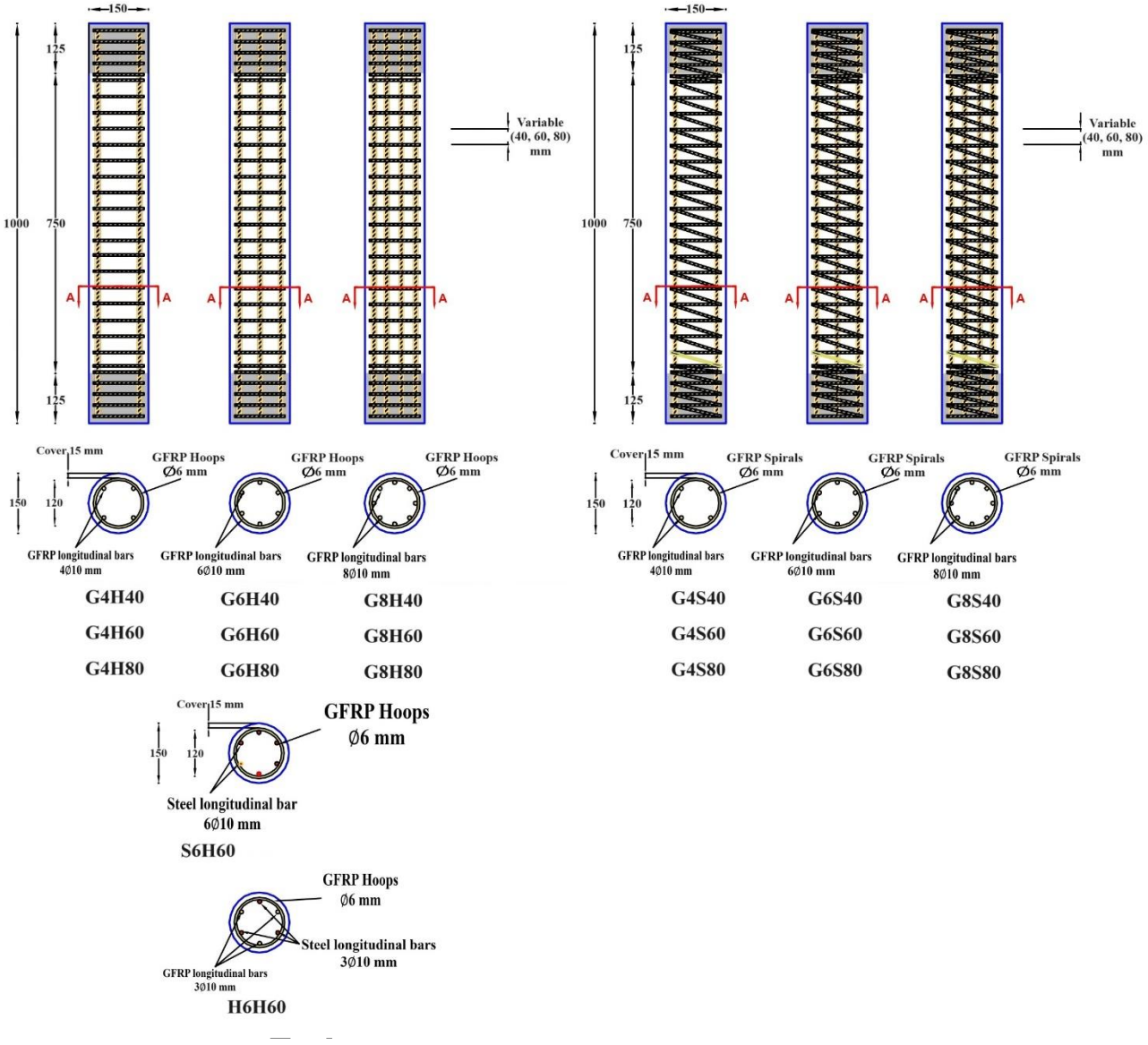

Figure 4. Reinforcement details and dimensions of the specimens.

The first letters, G, S, and H identify specimens reinforced with GFRP, steel, and hybrid (GFRP and steel) bars, respectively. The second letters, H and S, refer to the transverse reinforcement configuration (hoops and spirals). The left number in the specimen identification code indicates the number of longitudinal bars. The right number refers to the spacing between the transverse reinforcement. Both control specimens were reinforced transversely with 6 mm rounded GFRP #2 hoops with a spacing of 60mm. All specimens were designed in accordance with ACI code 440.22 [17] and CAN/CSA S807-19 [15] specifications.

All specimens were cast vertically to simulate typical construction practices with columns. The concrete was placed in the mold in three equal layers.

Table 4. The test matrix and reinforcement details.

Column's designations		Longitudinal Reinforcement			Transverse Reinforcement			
		Material type	No. & Size (mm)	ρ_l%	Material type	Size (mm)	Spacing (mm)	ρ_t%
G1	G4-H40	GFRP bars	4ϕ10	1.77	GFRP hoops	ϕ6	40	2.48
	G6-H40		6ϕ10	2.66				
	G8-H40		8ϕ10	3.55				
G2	G4-H60	GFRP bars	4ϕ10	1.77	GFRP hoops	ϕ6	60	1.65
	G6-H60		6ϕ10	2.66				
	G8-H60		8ϕ10	3.55				
G3	G4-H80	GFRP bars	4ϕ10	1.77	GFRP hoops	ϕ6	80	1.24
	G6-H80		6ϕ10	2.66				
	G8-H80		8ϕ10	3.55				
G4	G4-S40	GFRP bars	4ϕ10	1.77	GFRP spirals	ϕ6	40	2.48
	G6-S40		6ϕ10	2.66				
	G8-S40		8ϕ10	3.55				
G5	G4-S60	GFRP bars	4ϕ10	1.77	GFRP spirals	ϕ6	60	1.65
	G6-S60		6ϕ10	2.66				
	G8-S60		8ϕ10	3.55				
G6	G4-S80	GFRP bars	4ϕ10	1.77	GFRP spirals	ϕ6	80	1.24
	G6-S80		6ϕ10	2.66				
	G8-S80		8ϕ10	3.55				
Reference group	S6-H60	Steel bars	6ϕ10	2.66	GFRP hoops	ϕ6	60	1.65
	H6-H60	GFRP & Steel bars	3ϕ10 GFRP bars & 3ϕ10 steel bars					

4. Test setup and instrumentation

Four strain gauges were installed on the longitudinal and transverse reinforcement to measure the strains in the reinforcement during testing. In addition, one strain gauge was installed on the concrete surface at mid-height of the columns in the longitudinal direction to measure concrete strain. The location of internal instrumentation is illustrated in Fig. 5. Moreover, a linear variable differential transformer (LVDT) was used to measure the columns' total axial and lateral deformations. The location of external instrumentation is illustrated in Fig. 6. Two steel caps were used to confine both ends of the columns to prevent premature failure at the ends due to high stresses and to permit pin-pin boundary conditions. Steel caps measuring 150 mm in internal diameter and 8 mm in thickness. The steel cap is fixed on the top and bottom 125 mm portions of the column specimen. The typical schematic of the steel cap configuration is shown in Fig. 7. The axial loads were applied using a 3000 kN testing machine. The load is applied progressively in increments of 10 kN up to failure. During the test, load, and all deformations (strains and displacements), were automatically recorded and stored using a data-acquisition system (DAQ) connected to the computer. The typical schematic test setup for the concentrically loaded columns is shown in Fig. 8. Also, the load cell was used to measure the axial compression load of the specimen subjected to press forces using the electric compressive machine. Furthermore, all measurement instruments were connected to an electric data logger. The strain readings were recorded using a software program (DIAdem 2022 Q4).

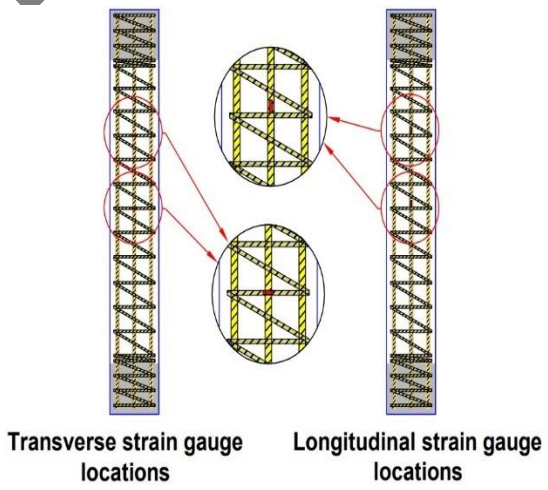

Figure. 5. The location of external instrumentation.

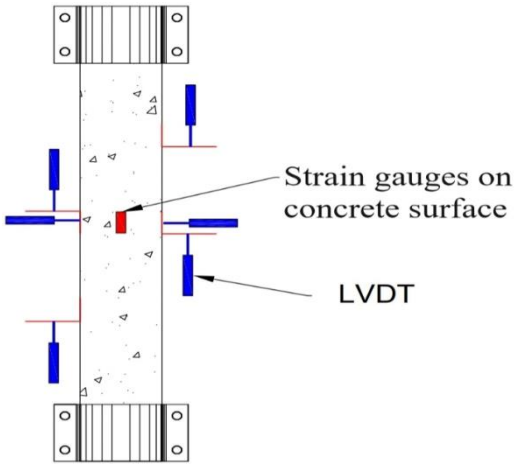

Figure 6. The location of internal instrumentation.

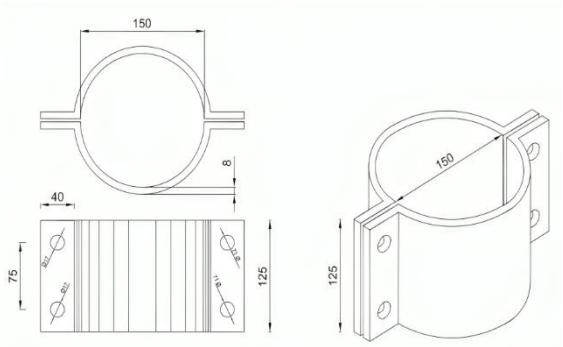

Figure 7. The typical schematic of the steel cap configuration.

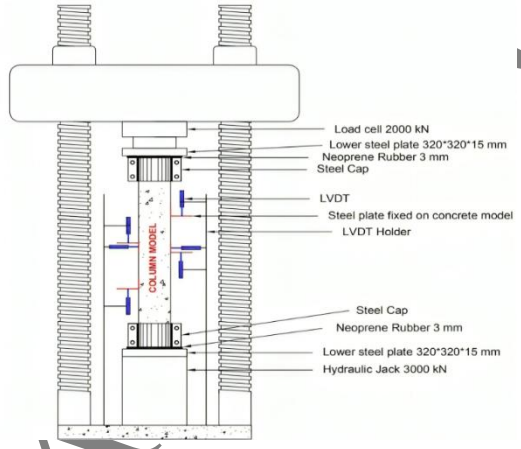

Figure 8. The typical schematic test setup.

5. Experimental results and discussions

5.1. General behavior and Failure modes

The GFRP-RPC specimens reinforced with GFRP spirals showed higher load capacity compared to GFRP-RPC specimens reinforced with GFRP hoops. For example, specimen G8-S40 provided a load capacity of 1653.2 kN, while specimen G8-H40 had a load capacity of 1409.7 kN, indicating an increase of 17.27% compared to its hoop-reinforced counterpart. The load capacity of GFRP-RPC specimens reinforced with GFRP spirals was higher than that of GFRP-RPC specimens reinforced with GFRP hoops, ranging from 9.95% to 18%. The longitudinal reinforcement ratio affected load capacity. An increase in longitudinal reinforcement led to an increase in load capacity in GFRP-RPC specimens. For example, specimen G8-H40 had a load capacity 46.5% higher than specimen G4-H40, and specimen G8-S40 had a load capacity 56.25% higher than specimen G4-S40. Furthermore, the spacing of transverse reinforcement affected load capacity. A decrease in transverse reinforcement spacing led to an increase in load capacity in GFRP-RPC specimens. For instance, specimen G8-H80 had a load capacity 9.13% lower than specimen G8-H40, and specimen G8-S80 had a load capacity 9.61% lower than specimen G8-S40. Regarding reference columns, specimens S6-H60 and H6-H60 had load capacities 19.45% and 14.61% higher, respectively, compared to specimen G6-H60. This can be attributed to the brittle nature of GFRP bars in the GFRP-RPC specimen compared to the ductile nature of the steel in the Steel-RPC and Hybrid-RPC specimens. The experimental test results are illustrated in Table 5. On the other hand, the type of longitudinal reinforcement (GFRP, Steel, and Hybrid), the type of transverse reinforcement (Hoops and Spirals), the longitudinal reinforcement ratio, and the transverse reinforcement ratio were the key factors that influenced the failure mode. During the testing of column specimens, it was observed that most columns exhibited very similar behavior during various stages of loading. Upon reaching the peak load, a catastrophic failure that was sudden, explosive, and unexpected was observed in all specimens. In contrast to other types of concrete in previous studies, this particular concrete type used in the current study and the type of reinforcement used did not show any structural failure indicators such as cracks or crack development during loading stages. However, some spalling of the concrete cover occurred in some columns as the loading progressed, which was more prominent in columns that exhibited high ductility and high load capacity. The separation of the concrete cover has contributed to activating the role of transverse reinforcement in providing confinement to the concrete core. The prominent indicator observed in all columns was the sound of reinforcement rupturing with increasing load, occurring before reaching the peak load. It may be interpreted as the reinforcement debonding from the concrete and rupturing within the concrete core before the final failure occurs. The sound intensified as the loading progressed and became more pronounced as the peak load approached. After reaching the peak load, a rapid decrease in load readings from the testing machine and the load cell was observed, along with rapid and explosive deformation, leading to sudden and unexpected failure, posing a danger to the column's integrity. Additionally, extremely high noise was heard, with scattered and powdered concrete parts dispersing in all directions at the moment of failure. It was observed that all the specimens failed in their upper or mid-half region, suggesting the effectiveness of the design and construction procedure employed in the study. The concentric compression load induced longitudinal strains that yielded transverse tensile strains. Following the spalling of the concrete cover, the concrete core experienced severe cracking and lateral expansion. Spiral reinforcement columns are distinguished by a more efficient failure mode and higher performance indicators compared to their hoop reinforcement counterparts. This can be attributed to the strong confinement provided by GFRP spirals compared to GFRP hoops, which helps maintain the integrity of longitudinal bars and concrete core for a longer period before failure occurs.

(A). First group (G1).

(B). Second group (G2).

(C). Third group (G3).

(D). Fourth group (G4)

(E). Fifth group (G5)

(F). Sixth group (G6).

(G). Seventh group (Reference Specimens).

Figure 9. Failure Mode of Column Specimens.

In contrast, hoop columns exhibited a failure mode characterized by the lateral movement of longitudinal bars, their rupturing, and the splitting of the concrete core in some specimens. Also, columns with higher reinforcement ratios showed higher failure indications than their counterparts. In the initial stages, deformations remained within the elastic range, but after increasing the applied load, the sound of reinforcement cracking was heard significantly. In some columns, slight spalling of the concrete cover occurred as the column bulged and shortened due to the distribution of internal stresses resulting from the applied loads. The damage to GFRP spirals was less severe than the damage to GFRP hoops, while most of the longitudinal GFRP bars experienced rupturing.

(G). Seventh group (Reference Specimens).The occurrence of longitudinal bars kinking and then delaminating in columns with a high transverse reinforcement ratio can be explained by the close spacing that restricts the lateral movement of the bars. Furthermore, both hoops and spirals incurred less damage as the transverse reinforcement ratio decreased, possibly due to the even distribution of stresses despite their failure at lower loads. Regarding the reference columns, the steel column specimen has retained the integrity of all GFRP hoops while experiencing buckling in all the longitudinal steel bars. On the other hand, in the hybrid column specimen, only one hoop ruptured, and there was buckling in all of its longitudinal steel bars, as well as rupturing in all the longitudinal GFRP bars. The columns' failure modes after the end of the tests are illustrated in Fig. 9.

Table 5. The experimental test results.

Group	ID specimens	Measured Results at Peak Load					Concrete Strains ε_c (με)	Bar Contribution		D.I. $(\frac{A_{\delta_{85}}}{A_{\delta_{75}}})$
		Load (kN)	Displacement (mm)		Reinforcement Strains					
		$P_{exp.}$ (kN)	δ_a (mm)	δ_l (mm)	ε_{bar} (με)	ε_t (με)		P_{bar} (kN)	$\frac{P_{bar}}{P_{exp.}}$ (%)	
G1	G4-H40	962.2	5.18	0.49	1968	255	1589	26	2.7	1.83
	G6-H40	1189.8	2.86	1.04	2250	288	1934	44	3.7	2.21
	G8-H40	1409.7	2.52	1.28	2477	326	2239	65	4.6	2.89
G2	G4-H60	910.5	3.96	1.20	1457	123	730	19	2.1	1.54
	G6-H60	1130.8	4.77	2.72	1322	141	656	26	2.3	1.96
	G8-H60	1328.3	4.30	2.91	1275	121	625	33	2.5	2.44
G3	G4-H80	875.4	4.48	1.48	1098	111.5	1048	14	1.6	1.30
	G6-H80	999	4.08	1.71	1198	134	1096	24	2.4	1.67
	G8-H80	1280.9	3.59	2.10	1371	101	1250	36	2.8	2.10
G4	G4-S40	1058	3.32	1.57	1967	14.1	1301	25.8	2.4	1.90
	G6-S40	1356.2	4.31	1.78	1885	12.2	1106	37.1	2.7	2.39
	G8-S40	1653.2	3.11	2.86	1614	11.7	1054	42.3	2.6	3.05
G5	G4-S60	1025	3.53	1.97	2091	14.1	1037	27.4	2.7	1.63
	G6-S60	1283.5	3.67	1.77	1819	12.0	871	35.8	2.8	2.04
	G8-S60	1509	4.73	1.46	1725	10.9	766	45.2	3.0	2.69
G6	G4-S80	1006.3	3.78	1.71	1979	13.5	958	25.9	2.6	1.34
	G6-S80	1178.8	4.04	1.73	1930	11.3	1002	38.0	3.2	1.72
	G8-S80	1494.2	4.58	1.80	1705	12.5	1380	44.7	3.0	2.18
Ref.	S6-H60	1350.8	5.15	2.37	1673	113	894	158	11.7	1.50
	H6-H60	1296.1	5.47	2.39	1615	250	571	16	1.2	1.63

* δ_a= axial displacement; δ_l= lateral displacement; D.I represent the ductility index.

5.2. Load–Axial Displacement Response

The typical load-axial displacement response for all column groups is illustrated in Fig. 10 to Fig. 15. The axial displacements were measured using four LVDTs, as shown in Fig. 5. Additionally, the corresponding axial displacements to their applied loads ($P_{exp.}$) were presented in Table 5. For the first group, the axial displacements for specimens G6-H40 and G8-H40 were 2.17 and 1.68 mm, respectively, representing a reduction of 58.12 and 67.59 %, respectively, compared to the axial displacement of specimen G4-H40 which is equal to 5.18 mm at the same load level (962.2 kN). For the second group, the axial displacements for specimens G6-H60 and G8-H60 were 3.51 and 3.38 mm, respectively, indicating a reduction of 11.25 and 14.67 %, respectively, compared to the axial displacement of specimen G4-H60 which is equal to 3.96 mm at the same load level (910.5 kN). For the third group, the axial displacements for specimens G6-H80 and G8-H80 were 3.02 and 1.72 mm, respectively, showing a reduction of 32.51 and 61.5 %, respectively, compared to the axial displacement of specimen G4-H80 which is equal to 4.48 mm at the same load level (875.4 kN). For the fourth group, the axial displacements for specimens G6-S40 and G8-S40 were 3.11 and 2.31 mm, respectively, reflecting a reduction of 6.35 and 30.36 %, respectively, compared to the axial displacement of specimen G4-S40 which is equal to 3.32 mm at the same load level (1058 kN). For the fifth group, the axial displacements for specimens G6-S60 and G8-S60 were 2.74 and 2.03 mm, respectively, signifies a reduction of 22.19 and 42.57 %, respectively, compared to the axial displacement of specimen G4-S60 which is equal to 3.53 mm at the same load level (1025 kN). For the sixth group, the axial displacements for specimens G6-S80 and G8-S80 were 3.07 and 2.74 mm, respectively, constituting a reduction of 18.89 and

27.54 %, respectively, compared to the axial displacement of specimen G4-S80 which is equal to 3.78 mm at the same load level (1006.3 kN). In general, the behavior of GFRP-RPC columns exhibited ascending linear behavior until reaching the maximum load. This was expected at this stage, as the column behavior was primarily governed by the well-known linear compressive properties of RPC, with a minor contribution from GFRP bars. After reaching the maximum load, the concrete cover of all columns spalled explosively without visible cracks, significantly reducing and sudden the load capacity. Interestingly, it was observed that the capacity of the columns remained almost similar after failure and crushing, with a rapid decline in load capacity. This behavior can be attributed to the efficiency of GFRP hoops and GFRP spirals (due to their tension) and GFRP bars (due to rupture or buckling) and their influence on the load capacity, which will be further discussed. Despite four hoop columns (G6-H40, G8-H40, G8-H60, and G8-H80) showing superior stiffness compared to their spiral counterparts, most of the spiral columns were stiffer (with lesser axial deformations) than the hoop columns. It can be observed that the G8-H40 specimen exhibited the highest stiffness among all hoop columns, and similarly, the G8-S40 specimen displayed the highest stiffness among all spiral columns. This can be attributed to the fact that these two specimens had higher reinforcement ratios (both longitudinally and transversely), resulting in increased stiffness and reduced deformations. Reducing the spacing of hoops and the pitches of spirals led to an increase in failure load and a decrease in axial displacement. The increased displacement in some spiral columns can be explained due to the additional confinement effect leading to increased failure load and catastrophic rupturing of the spirals compared to the hoop columns. In addition, the G4-H40 specimen exhibited the maximum axial displacement at the peak load. This may be attributed to the delay in the activation of confinement before reaching ultimate failure, where the longitudinal bars could not mitigate the development of deformations, leading to their rupturing and splitting of the concrete core.

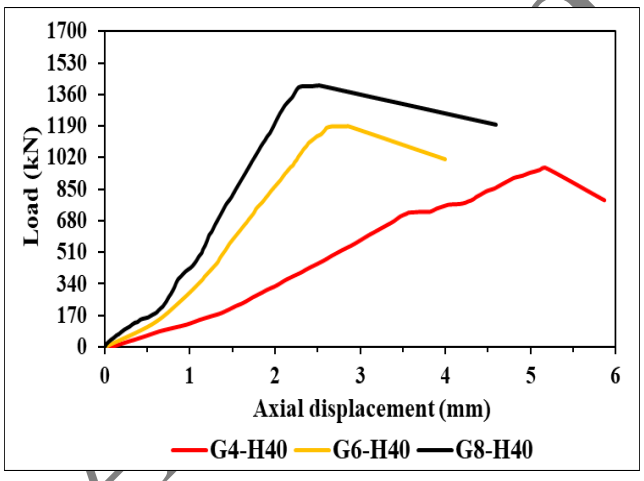

Figure 10. Load-Axial displacement for G1

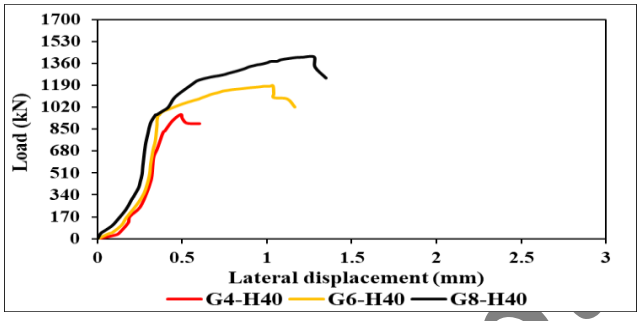

Figure 11. Load-Axial displacement for G2.

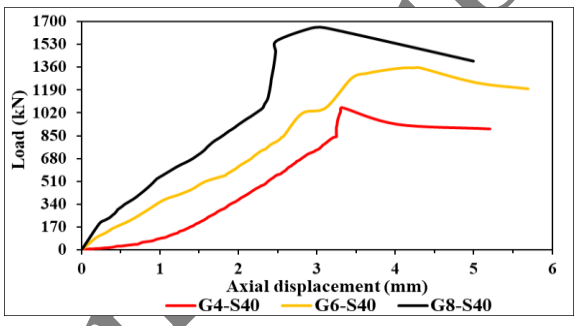

Figure 12. Load-Axial displacement for G3.

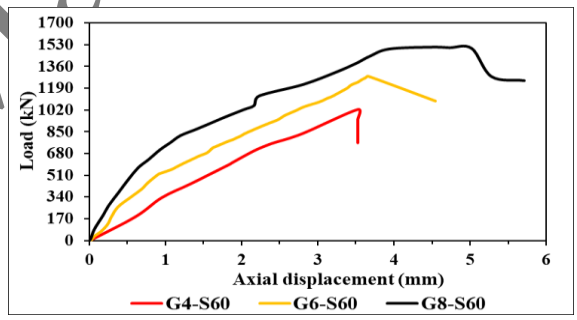

Figure 13. Load-Axial displacement for G4.

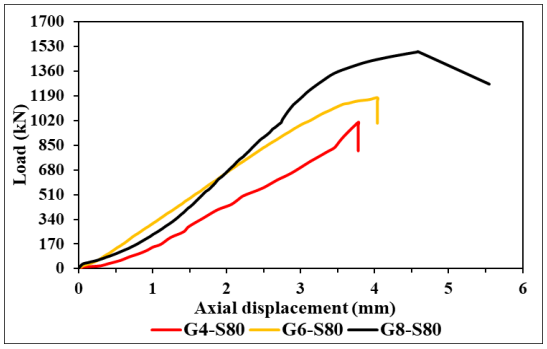

Figure 14. Load-Axial displacement for G5.

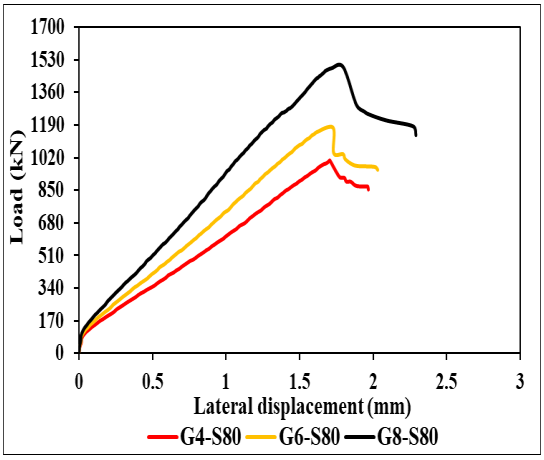

Figure 15. Load-Axial displacement for G6.

5.3. Load–Lateral Displacement Response

The typical load-lateral displacement response for all column groups is illustrated in Fig. 16 to Fig. 21. The lateral displacements were measured using three LVDTs, as shown in Fig. 5. For the first group, the lateral displacements for specimens G6-H40 and G8-H40 were 0.36 and 0.35 mm, respectively, representing a reduction of 25.68 and 28.78 %, respectively, compared to the lateral displacement of specimen G4-H40 which is equal to 0.49 mm at the same load level (962.2 kN). For the second group, the lateral displacements for specimens G6-H60 and G8-H60 were 0.88 and 0.87 mm, respectively, indicating a reduction of 26.09 and 27.65 %, respectively, compared to the lateral displacement of specimen G4-H60 which is equal to 1.2 mm at the same load level (910.5 kN). For the third group, the lateral displacements for specimens G6-H80 and G8-H80 were 1.43 and 1.25 mm, respectively, showing a reduction of 3.38 and 15.25 %, respectively, compared to the lateral displacement of specimen G4-H80 which is equal to 1.48 mm at the same load level (875.4 kN). For the fourth group, the lateral displacements for specimens G6-S40 and G8-S40 were 1.5 and 1.34 mm, respectively, reflecting a reduction of 4.44 and 14.71 %, respectively, compared to the lateral displacement of specimen G4-S40 which is equal to 1.57 mm at the same load level (1058 kN). For the fifth group, the lateral displacements for specimens G6-S60 and G8-S60 were 1.17 and 0.67 mm, respectively, signifies a reduction of 40.48 and 66 %, respectively, compared to the lateral displacement of specimen G4-S60 which is equal to 1.97 mm at the same load level (1025 kN). For the sixth group, the lateral displacements for specimens G6-S80 and G8-S80 were 1.37 and 1.07 mm, respectively, constituting a reduction of 19.4 and 37.35 %, respectively, compared to the lateral displacement of specimen G4-S80 which is equal to 1.71 mm at the same load level (1006.3 kN). Based on the results, it is evident that GFRP-RPC specimens were not subjected to significant lateral deformations before failure, exhibiting values ranging between 0.49 and 2.91 mm. This can be attributed to the test being concentric and the absence of eccentricities, in addition to the specimen's ideal positioning at the center of the testing apparatus. Furthermore, the ultra-strength of RPC against deformations contributed to this behavior. The linear increase in lateral deformations with increasing load can be explained due to the stress of hoops and spirals before fracturing due to the bond failure between the interface of GFRP bars and RPC, resulting in increased applied loads, which led to the expansion of the concrete core. This bond plays a crucial role in specimen expansion and preserving the concrete core against deformations. Furthermore, all groups (except G5) showed an increase in lateral deformations with an increase in the longitudinal reinforcement ratio where specimens failed under high central loads, resulting in higher lateral dilation compared to specimens with lower longitudinal reinforcement ratios in each group. Moreover, most of the spiral specimens exhibited higher lateral deformations than their hoop counterparts (except G6-S60, G8-S60, and G8-S80) due to their capacity to carry higher loads, leading to increased dilation. Additionally, G4 specimens exhibited greater deformations compared to G1 specimens due to the increased applied loads and delayed activation of concrete core confinement to carry stresses. This resulted in clear buckling and rupturing of the bars and spirals, as well as further RPC crushing. G4-H40 specimens showed lesser deformations compared to the hoop specimens with the same longitudinal reinforcement ratio (G4-H60 and G4-H80) because the GFRP bars continued to carry loads without early buckling or rupturing due to closely spaced hoops.

5.4. Longitudinal Compressive Strains (ε_{bar})

The typical relationships between the load and the longitudinal compression strains in the longitudinal bars for all column groups are shown in Fig. 22 to Fig. 27. The longitudinal strains were measured using four strain gauges, as shown in Fig. 6. Additionally, the longitudinal strains at the peak load (ε_{bar}) are summarized in Table 5. For the first group, the longitudinal strains for specimens G6-H40 and G8-H40 were 1502 and 1397 μ_ε, respectively, representing a reduction of 23.7 and 29%, respectively, compared to the longitudinal strain of specimen G4-H40 which is equal to 1968 μ_ε at the same load (962.2 kN). For the second group, the longitudinal strains for specimens G6-H60 and G8-H60 were 1243 and 1006 μ_ε, respectively, representing a reduction of 14.7 and 31%, respectively, compared to the longitudinal strain of specimen G4-H60 which is equal to 1457 μ_ε at the same load (910.5 kN). For the third group, the longitudinal strains for specimens G6-H80 and G8-H80 were 1054 and 927 μ_ε, respectively, representing a reduction of 3.96 and 15.54%, respectively, compared to the longitudinal strain of specimen G4-H80 which is equal to 1098 μ_ε at the same load (875.4 kN). For the fourth group, the longitudinal strains for specimens G6-S40 and G8-S40 were 1401 and 968 μ_ε, respectively, reflecting a reduction of 28.8 and 50.81 %, respectively, compared to the longitudinal strain of specimen G4-S40 which is equal to 1967 μ_ε at the same load level (1058 kN). For the fifth group, the longitudinal strains for specimens G6-S60 and G8-S60 were 1430 and 1145 μ_ε, respectively, signifies a reduction of 31.61 and 45.27 %, respectively, compared to the longitudinal strain of specimen G4-S60 which is equal to 2091 μ_ε at the same load level (1025 kN). For the sixth group, the longitudinal strains for specimens G6-S80 and G8-S80 were 1582 and 1077 μ_ε, respectively, constituting a reduction of 20.1 and 45.6 %, respectively, compared to the longitudinal strain of specimen G4-S80 which is equal to 1979 μ_ε at the same load level (1006.3 kN). All the specimens behaved similarly until failure occurred, exhibiting a relatively linear ascending response behavior in the load-longitudinal strain curves in the ascending part even reaching peak load, indicating that the behavior at this stage was primarily associated with concrete.

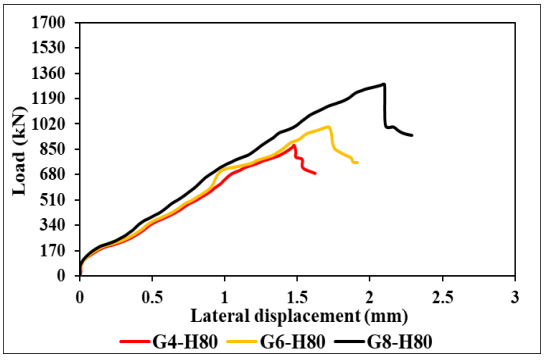

Figure 16. Load-Lateral displacement for G1.

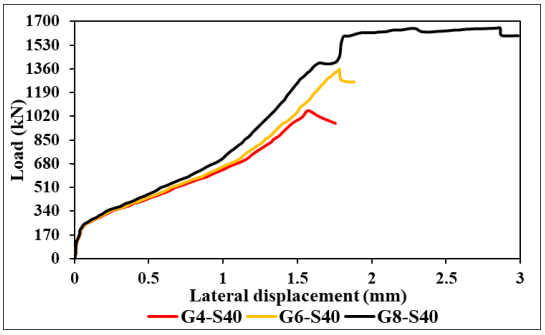

Figure 17. Load-Lateral displacement for G2.

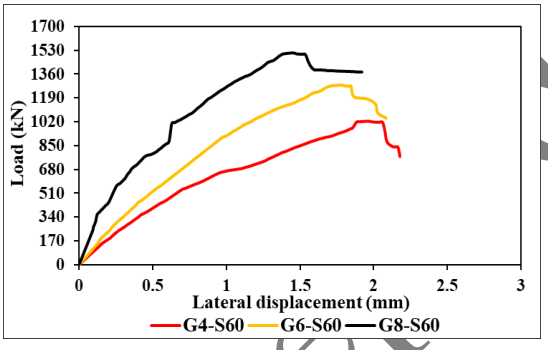

Figure 18. Load-Lateral displacement for G3.

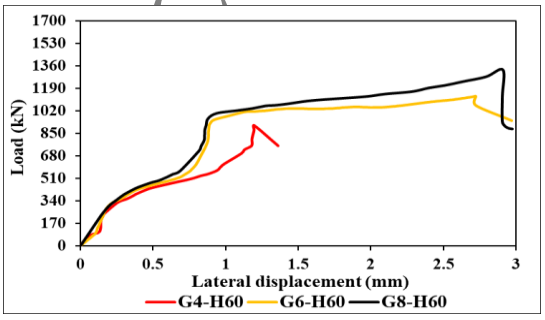

Figure 19. Load-Lateral displacement for G4

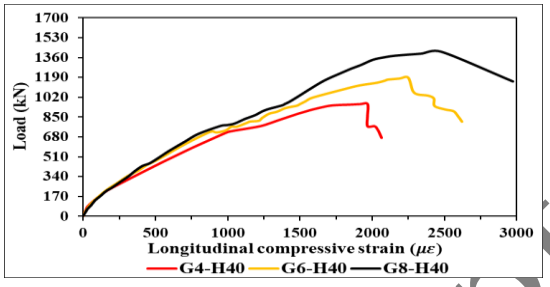

Figure 20. Load-Lateral displacement for G5.

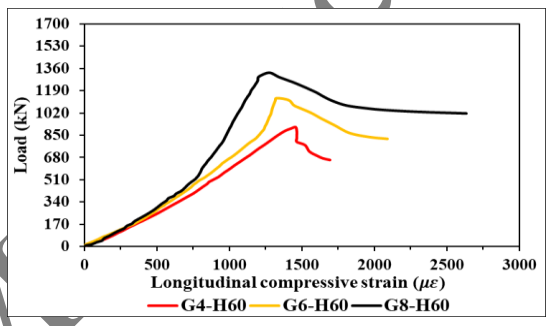

Figure 21. Load-Lateral displacement for G6.

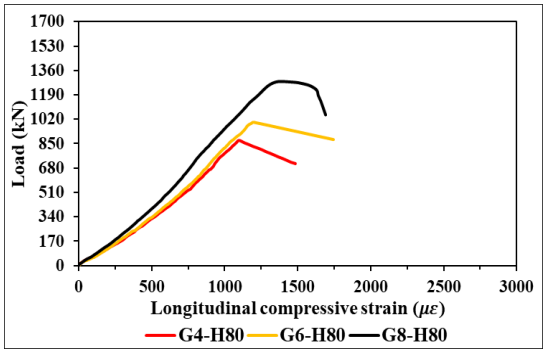

Figure 22. Load-Longitudinal strain for G1

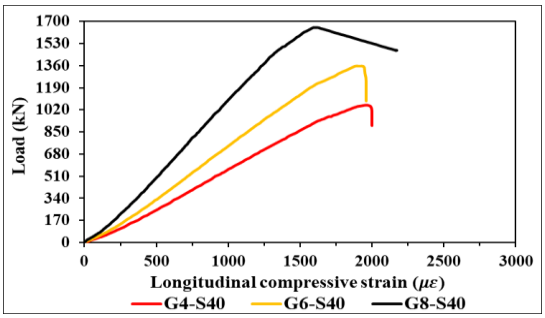

Figure 23. Load-Longitudinal strain for G2

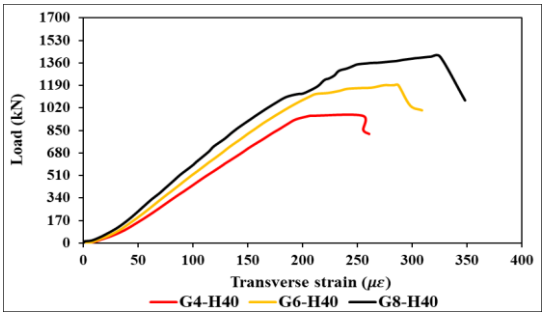

Figure 24. Load-Longitudinal strain for G3.

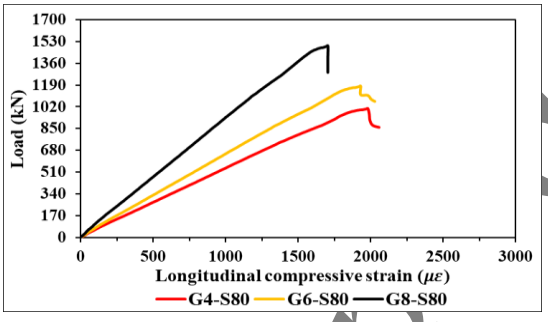

Figure 25. Load-Longitudinal strain for G4...

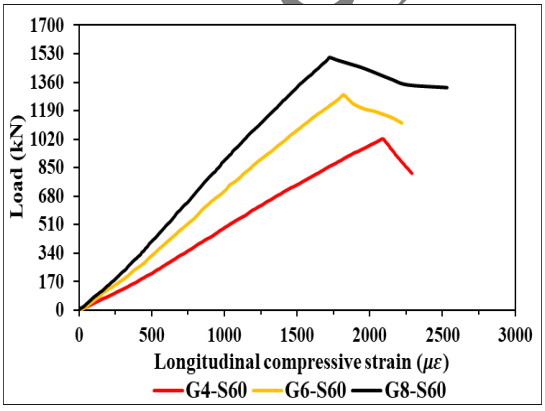

Figure 26. Load-Longitudinal strain for G5.

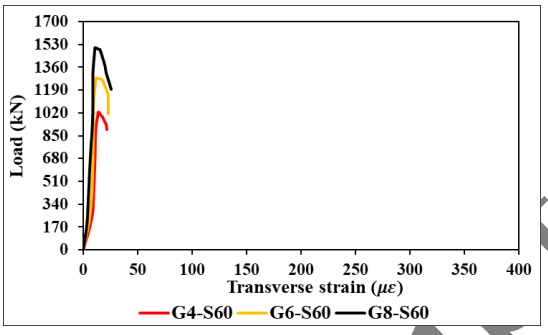

Figure 27. Load-Longitudinal strain for G6.

The peak load and the corresponding longitudinal strain varied from one specimen to another depending on the core confinement properties. The compressive strain values for the spiral specimens ranged from 1614 to 2091 μ_ε (with an average value of 1857 μ_ε) and ranged from 1098 to 2477 μ_ε for hoop specimens (with an average value of 1602 μ_ε). This suggests that the average peak strain of spiral specimens was higher by 15.95% compared to hoop specimens, even though the maximum recorded value was for a hoop specimen (G8-H40), supporting the idea that spirals provide better confinement than hoops, aiding longitudinal bars to better load capacity [2, 31-36]. Thus, the spiral specimens have greater stiffness than hoop specimens. Furthermore, the results showed that GFRP bars maintained their integrity and resistance to loading until the surrounding concrete was crushed and fragmented upon reaching the peak load, resulting in a clear rupture and buckling for GFRP bars. The post-peak curves for the load-longitudinal strain diagrams experienced a rapid drop for most of the specimens. It is noteworthy that the compressive strain of GFRP longitudinal bars for some specimens (G6-H40, G8-H40, and G4-S60) exceeded the allowable strain limit of 2000 μ_ε recommended by CSA S807-19 [8] for calculating the nominal capacity of GFRP-reinforced columns. As a result, these specimens experienced more significant deterioration due to the buckling or rupture of their longitudinal, hoop, and spiral bars, accompanied by the crushing and fragmentation of concrete at the moment of explosive failure. Additionally, the well-confined G8-H40 specimen exhibited the highest value (ε_{bar}) among all specimens, equivalent to 2477 μ_ε or 13.78% of the ultimate tensile strain of GFRP bars (ε_f) reported by the manufacturer, which aligns with the recommendation in ACI 440-22 [10], which states that "for design purposes, at peak load for test specimens, the maximum strain in GFRP bars should not exceed 50% of the maximum tensile strain in GFRP bars".

5.5. Transverse Reinforcement Strain (ε_t)

The typical relationships between the load and the transverse strains in GFRP hoops and spirals for all column groups are shown in Fig. 28 to Fig. 33. The transverse strains were measured using two strain gauges, as shown in Fig. 6. Additionally, the transverse strains at the peak load (ε_t) are summarized in Table 5. For the first group, the transverse strains for specimens G6-H40 and G8-H40 were 175 and 157 μ_ε, respectively, representing a reduction of 31.2 and 38.5%, respectively, compared to the transverse strain of specimen G4-H40 which is equal to 255 μ_ε at the same

load (962.2 kN). For the second group, the transverse strains for specimens G6-H60 and G8-H60 were 82.54 and 70.5 μ_ε, respectively, representing a reduction of 32.7 and 42.5 %, respectively, compared to the transverse strain of specimen G4-H60 which is equal to 123 μ_ε at the same load (910.5 kN). For the third group, the transverse strains for specimens G6-H80 and G8-H80 were 90.6 and 76.2 μ_ε, respectively, representing a reduction of 18.7 and 31.64%, respectively, compared to the transverse strain of specimen G4-H80 which is equal to 111.5 μ_ε at the same load (875.4 kN). For the fourth group, the transverse strains for specimens G6-S40 and G8-S40 were 9.75 and 8.78 μ_ε, respectively, reflecting a reduction of 30.76 and 37.7 %, respectively, compared to the transverse strain of specimen G4-S40 which is equal to 14.11 μ_ε at the same load level (1058 kN). For the fifth group, the transverse strains for specimens G6-S60 and G8-S60 were 9.5 and 8.83 μ_ε, respectively, signifies a reduction of 32.6 and 37.28 %, respectively, compared to the transverse strain of specimen G4-S60 which is equal to 14.09 μ_ε at the same load level (1025 kN). For the sixth group, the transverse strains for specimens G6-S80 and G8-S80 were 11.51 and 7.73 μ_ε, respectively, constituting a reduction of 14.95 and 42.91 %, respectively, compared to the transverse strain of specimen G4-S80 which is equal to 13.53 μ_ε at the same load level (1006.3 kN). The load-transverse strain curves of hoop GFRP-RPC specimens exhibited approximately linear ascending branches within a wide range until the peak load while the curves of spiral GFRP-RPC specimens also showed linear ascending branches but within a very narrow range. The tensile strains in the GFRP hoops of hoop GFRP-RPC specimens ranged from 101 to 326 μ_ε (with an average value of 178 μ_ε), while the tensile strains in the GFRP spirals of spiral GFRP-RPC specimens ranged from 10.9 to 14.1 μ_ε (with an average value of 12.5 μ_ε). The difference in the values of strains between the spiral and hoop specimens can be attributed to the different behavior of the longitudinal GFRP bars in spirals compared to hoops. It was observed that the spirals experienced catastrophic failure, with most of the bars in the spirals rupturing at the moment of failure, unlike longitudinal GFRP bars in the hoops. This can also be explained by the high confinement efficiency of the spirals, as spirals are continuous bars in contrast to hoops, which allowed them to act as a single bar against the tensile forces resulting from the expansion of the concrete core. Additionally, the fact that all the specimens were made using RPC, known for their ultra strength, contributed to providing additional transverse reinforcement support before reaching the peak load. The contribution of the confinement pressure of the hoops was provided early on, starting from the beginning of loading, as the responses of the hoops to the tensile forces caused them to expand early, leading to their rupture and the separation of the concrete core in several specimens. This is in contrast to the confinement pressure of the spirals, which was slightly affected by the expansion of the concrete core and exhibited very slight responses to the tensile forces, resulting in delayed expansion and maintaining the integrity of the concrete core.

5.6. Concrete Compressive Strains (ε_c)

The typical relationships between the load and the compressive strain responses of RPC for all column groups are shown in Fig. 34 to Fig. 39. The RPC strains were measured using one strain gauge at the midheight of the specimens, where the maximum compressive strain was anticipated, as shown in Fig. 5. Additionally, the RPC strains at the peak load (ε_c) are summarized in Table 5. For the first group, the RPC strains for specimens G6-H40 and G8-H40 were 1168 and 1117 μ_ε, respectively, representing a reduction of 26.5 and 29.7 %, respectively, compared to the RPC strain of specimen G4-H40 which is equal to 1589 μ_ε at the same load (962.2 kN). For the second group, the RPC strains for specimens G6-H60 and G8-H60 were 584 and 513 μ_ε, respectively, representing a reduction of 28.5 and 29.7 %, respectively, compared to the RPC strain of specimen G4-H60 which is equal to 730 μ_ε at the same load (910.5 kN). For the third group, the RPC strains for specimens G6-H80 and G8-H80 were 985 and 889 μ_ε, respectively, representing a reduction of 6 and 15.2 %, respectively, compared to the RPC strain of specimen G4-H80 which is equal to 1048 μ_ε at the same load (875.4 kN). For the fourth group, the RPC strains for specimens G6-S40 and G8-S40 were 872 and 667 μ_ε, respectively, reflecting a reduction of 33 and 48.72 %, respectively, compared to the RPC strain of specimen G4-S40 which is equal to 1301 μ_ε at the same load level (1058 kN). For the fifth group, the RPC strains for specimens G6-S60 and G8-S60 were 720 and 544 μ_ε, respectively, signifies a reduction of 30.6 and 47.6 %, respectively, compared to the RPC strain of specimen G4-S60 which is equal to 1037 μ_ε at the same load level (1025 kN). For the sixth group, the RPC strains for specimens G6-S80 and G8-S80 were 766 and 618 μ_ε, respectively, constituting a reduction of 20 and 35.47 %, respectively, compared to the RPC strain of specimen G4-S80 which is equal to 958 μ_ε at the same load level (1006.3 kN). The strain values of the RPC presented by the hoop GFRP-RPC specimens ranged from 625 to 2239 μ_ε (with an average value of 1241 μ_ε), while the strain values of the RPC presented by the spiral GFRP-RPC specimens ranged from 766 to 1380 μ_ε (with an average value of 1053 μ_ε). The results indicate that the hoop GFRP-RPC specimens with high confinement (40 mm) recorded higher strains compared to the other specimens, where the closely spaced GFRP hoops contributed to activating the lateral confinement restraint from the beginning of loading, resulting in the expansion and compression of the concrete core against the concrete cover. Concrete crushing was the dominant failure mode for most of the specimens, although some exhibited localized concrete spalling before reaching the peak load. The load-concrete strain curves for the GFRP-RPC specimens suggest that the curves were approximately linear up to around 85% of the failure load. At this point, there was a significant activation of lateral restraint provided by the hoops and spirals to confine the concrete core, leading to concrete spalling in some specimens. After reaching the peak load, the GFRP-RPC specimens lost a significant portion of their load capacity due to sudden and explosive concrete cover crushing. However, some specimens exhibited ductile behavior. The confinement pressure from the activated transverse reinforcement before the peak load contributed to the expansion of the concrete core. Nevertheless, several specimens exhibited mild strains when compared to other specimens, which may be attributed to greater deformations occurring in other regions of the concrete far, where a strain gauge is not present.

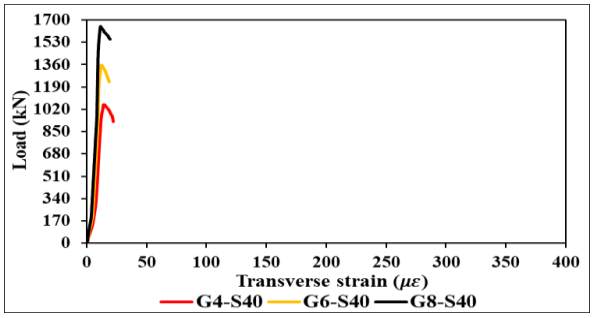

Figure 28. Load-Transverse strain for G1.

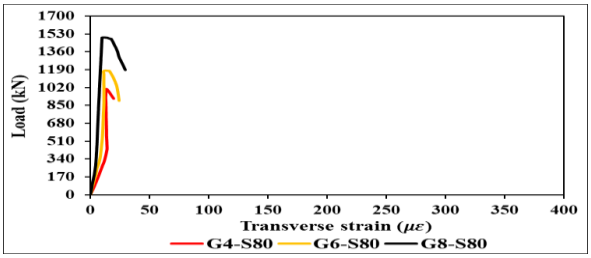

Figure 29. Load-Transverse strain for G2.

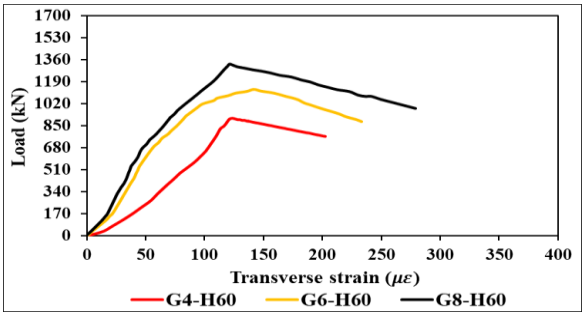

Figure 30. Load-Transverse strain for G3.

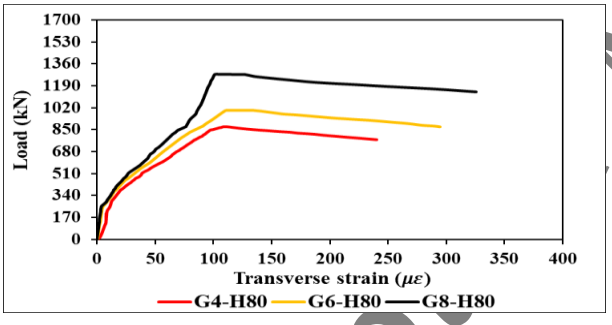

Figure 31. Load-Transverse strain for G4.

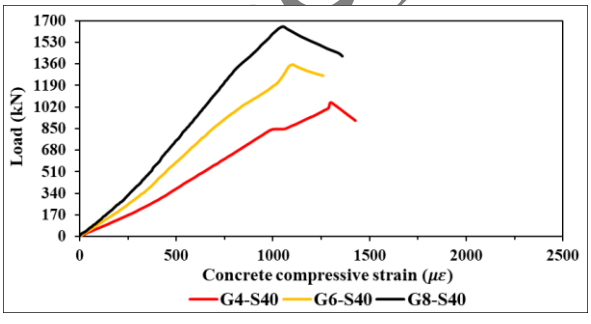

Figure 32. Load-Transverse strain for G5.

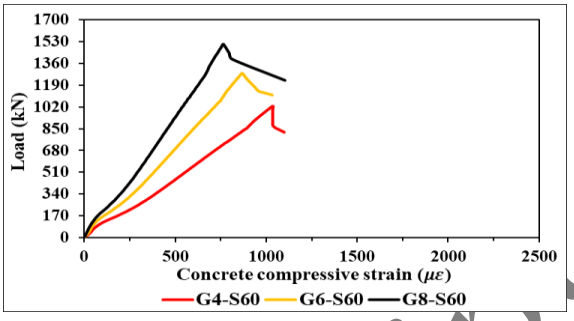

Figure 33. Load-Transverse strain for G6.

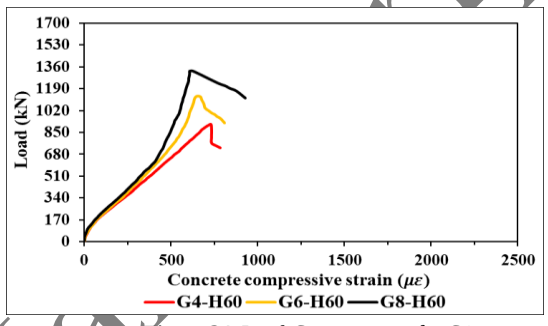

Figure 34. Load-Cocrete strain for G1.

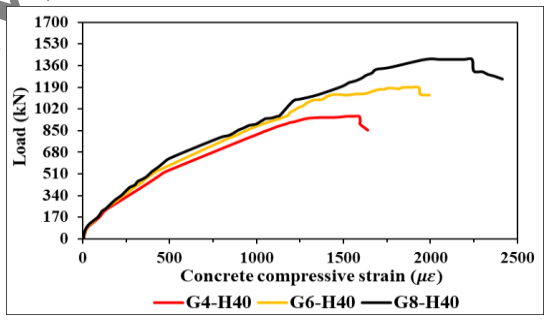

Figure 35. Load-Concrete strain for G2.

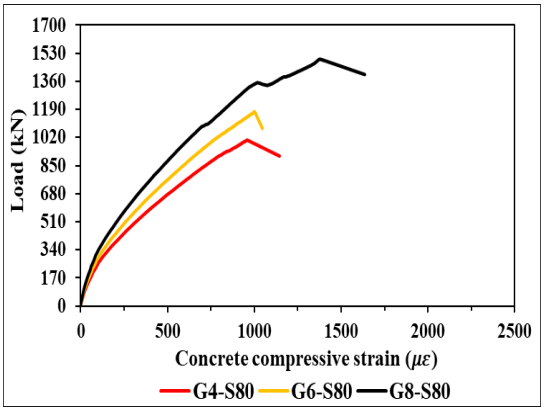

Figure 36. Load-Concrete strain for G3.

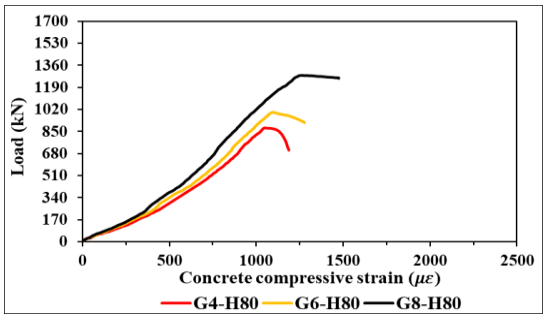

Figure 37. Load-Concrete strain for G4.

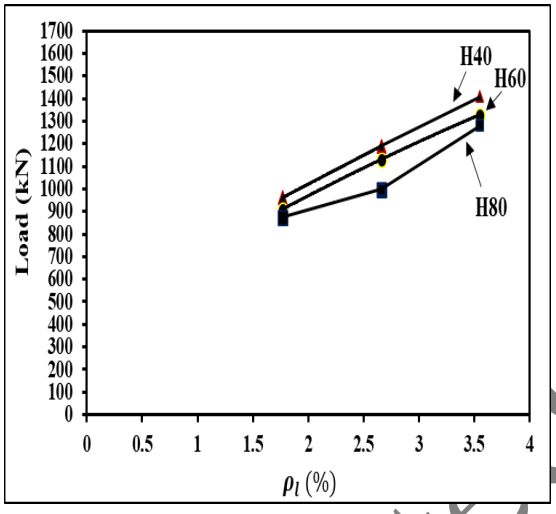

Figure 38. Load-Concrete strain for G5.

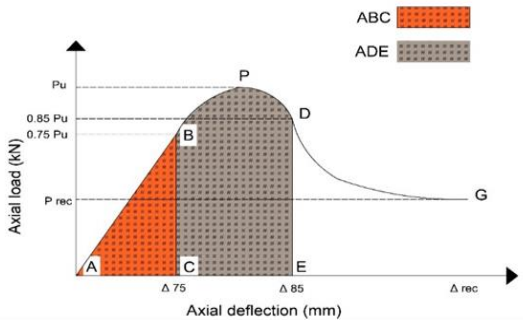

Figure 39. Load-Concrete strain for G6.

5.7. Ductility Index (D.I.)

The ductility can be described as the capacity of a structural member to absorb energy once the ultimate axial strength has been reached. This capacity can be expressed in terms of several parameters, including strain, deflection, rotation, absorbed energy, or dissipated energy of the members [37]. The ductility index (D.I.) for all specimens can be calculated using Equation (1) [37–39]:

$$D.I = A_{\delta 85}/A_{\delta 75} \quad (1)$$

Where $A_{\delta_{75}}$ represents the total are ofthe load-displacement curve in the elastic region up to the displacement (δ_{75}) corresponding to 75% of the ultimate load of the column (the area ABC), while $A_{\delta_{85}}$ is the total area of the load-displacement curve up to the axial displacement (δ_{85}) corresponding to 85% of the ultimate load of the column in the post-peak loading curve (the area ADE), as graphically presented in Fig. 40.

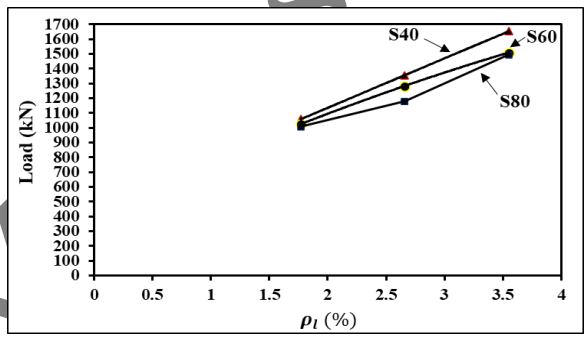

Figure 40. Graphical representation of ductility index [37].

The ductility index for all tested columns is summarized in Table 6 and Table 7. The overall behavior of GFRP-RPC columns was initially brittle, but this brittleness reduced as the longitudinal and transverse reinforcement increased. The G8-S40 specimen exhibited the highest ductility value (3.05), while the G4-H80 specimen had the lowest value (1.3). Furthermore, groups with higher confinement (G1 and G4) using GFRP hoops and spirals demonstrated superior ductility compared to other groups, attributed to effective confinement of the concrete core and nearly uniform compression by the hoops and spirals. The influence of the longitudinal reinforcement ratio on ductility is shown in Table 6. It was found that an increase in the longitudinal reinforcement ratio also contributed to improving the ductility index. For example, increasing the longitudinal reinforcement ratio from 1.77% to 3.55% for spiral GFRP-RPC specimens, increased the ductility mean by 62.74%. Similarly, increasing the longitudinal reinforcement ratio from 1.77% to 3.55% for hoop GFRP-RPC specimens, led to an increase in the ductility mean by 59.3%.

The effect of the transverse reinforcement ratio on ductility is shown in Table 7. It was found that increasing the transverse reinforcement ratio of GFRP-RPC specimens contributes to an increase in the ductility index. For example, when increasing the transverse reinforcement ratio of spiral GFRP-RPC specimens from 1.24% to 2.48%, the ductility means increases by 40.21%. Similarly, when increasing the transverse reinforcement ratio of hoop GFRP-RPC specimens from 1.24% to 2.48%, the ductility means increases by 36.9%. These results are consistent with what was found by

previous studies [2, 15, 18, 19, 33, 34, 36, 40–48] regarding reinforced concrete circular columns with GFRP bars and spirals or hoops.

Table 6. The effect of the longitudinal reinforcement ratio on ductility index.

Group	ID specimens	Measured Results at Peak Load	D.I. ($\frac{A_{\delta_{85}}}{A_{\delta_{75}}}$)	Difference (%)
		Ultimate Load (kN)		
		$P_{exp.}$ (kN)		
G1	G4-H40	962.2	1.83	-
	G6-H40	1189.8	2.21	+ 20.76
	G8-H40	1409.7	2.89	+ 57.92
G2	G4-H60	910.5	1.54	-
	G6-H60	1130.8	1.96	+ 27.27
	G8-H60	1328.3	2.44	+ 58.44
G3	G4-H80	875.4	1.30	-
	G6-H80	999	1.67	+ 28.46
	G8-H80	1280.9	2.10	+ 61.53
G4	G4-S40	1058	1.90	-
	G6-S40	1356.2	2.39	+ 25.79
	G8-S40	1653.2	3.05	+ 60.52
G5	G4-S60	1025	1.63	-
	G6-S60	1283.5	2.04	+ 25.15
	G8-S60	1509	2.69	+ 65
G6	G4-S80	1006.3	1.34	-
	G6-S80	1178.8	1.72	+ 28.35
	G8-S80	1494.2	2.18	+ 62.7
Ref.	S6-H60	1350.8	1.50	- 23.47 *
	H6-H60	1296.1	1.63	- 16.83 *

* Calculated compared to the ductility of the G6-H60 specimen.

Table 7. The effect of the transverse reinforcement ratio on ductility index.

Group	ID specimens	Measured Results at Peak Load	D.I. ($\frac{A_{\delta_{85}}}{A_{\delta_{75}}}$)	Difference (%)
		Ultimate Load (kN)		
		$P_{exp.}$ (kN)		
H80	G4-H80	875.4	1.30	-
	G4-H60	910.5	1.54	18.461
	G4-H40	962.2	1.83	40.769
H60	G6-H80	999	1.67	-
	G6-H60	1130.8	1.96	17.365
	G6-H40	1189.8	2.21	32.335
H40	G8-H80	1280.9	2.10	-
	G8-H60	1328.3	2.44	16.190
	G8-H40	1409.7	2.89	37.619
S80	G4-S80	1006.3	1.34	-
	G4-S60	1025	1.63	21.641
	G4-S40	1058	1.90	41.791
S60	G6-S80	1178.8	1.72	-
	G6-S60	1283.5	2.04	18.604
	G6-S40	1356.2	2.39	38.953
S40	G8-S80	1494.2	2.18	-
	G8-S60	1509	2.69	23.394
	G8-S40	1653.2	3.05	39.908

On the other hand, regarding the configuration of the transverse reinforcement, the spiral GFRP-RPC specimens demonstrated a more ductile behavior when compared to their hoop counterparts, with an average ductility index of 2.1 for all spiral specimens, while the average ductility index for all hoop specimens was 1.99. This can be attributed to the fact that spirals provide ideal confinement as spirals are continuous bars, effectively containing the concrete core for a longer duration before deformations occur, unlike the hoops which are discrete. Through the results, it is evident that the ductility of the GFRP-RPC specimen (1.96) is greater than that of the Steel-RPC specimen (1.5) because the GFRP-RPC specimen absorbs more energy through its flexibility and ability to well deforming in the post-peak collapse region. Furthermore, the Hybrid-RPC specimen exhibited less ductility (1.63) than the GFRP-RPC specimen (1.96) but more than the Steel-RPC specimen (1.5), which reinforces the though mentioned, indicating the existence of a distinct mechanism in the hybrid column that contributed to its superiority over the S6-H60 specimen. This can be attributed to the combined use of GFRP bars and hoops resulting in higher ductility, leading to a longer duration in the plastic zone. Based on the above results, it's evident that increasing the longitudinal reinforcement ratio has a greater effect on the ductility than the transverse reinforcement ratio.

6. Discussion

6.1. Influence of longitudinal reinforcement ratio

The low-reinforcement ratio specimens (1.77 %) failed in a brittle and explosive manner compared to the higher reinforcement ratio specimens (2.66 % and 3.55 %). Increasing the longitudinal reinforcement ratio from 1.77 to 2.66 % in the GFRP-RPC hoop specimens contributed to an increase in load capacity ranging from approximately 14.12 to 24.2 %. Increasing the longitudinal reinforcement ratio from 1.77 to 3.55 % in the GFRP-RPC hoop specimens contributed to an approximately 46 % increase in load capacity. Additionally, increasing the longitudinal reinforcement ratio from 1.77 to 2.66 % in the GFRP-RPC spiral specimens contributed to an increase in load capacity ranging from approximately 17.14 to 28.19 %. Increasing the longitudinal reinforcement ratio from 1.77 to 3.55 % in the GFRP-RPC spiral specimens contributed to an increase in load capacity ranging from approximately 47.22 to 56.25 %. The effect of the longitudinal reinforcement ratio on the ultimate load for hoop and spiral specimens is illustrated in Fig. 41 and Fig. 42, respectively.

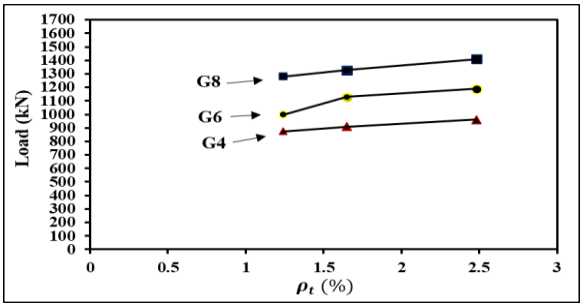

Figure 41. Effect of ρ_l on ultimate load for hoop specimens.

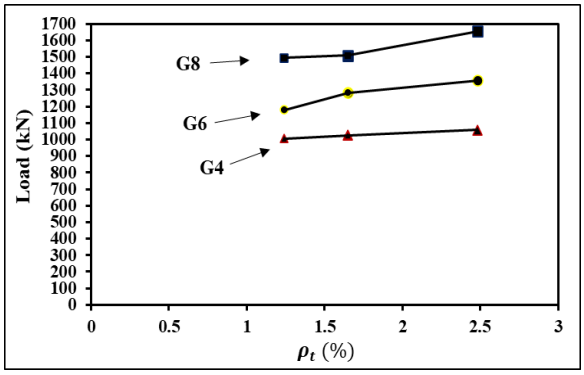

Figure 42. Effect of ρ_l on ultimate load for spiral specimens.

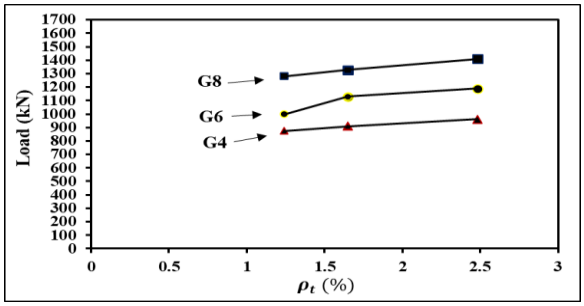

Figure 43. Effect of ρ_t on ultimate load for hoop specimens.

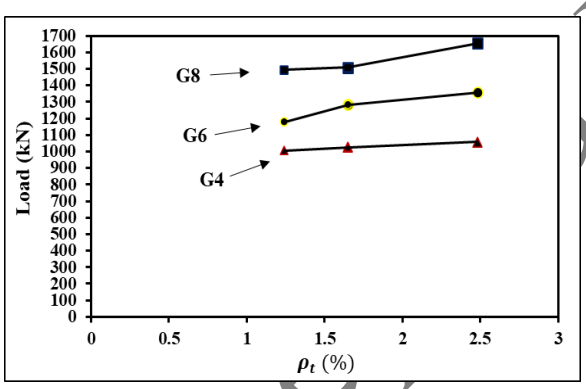

Figure 44. Effect of ρ_t on ultimate load for spiral specimens.

From the above results, it is evident that increasing the longitudinal reinforcement ratio significantly enhances load capacity. Furthermore, when increasing the longitudinal reinforcement ratio, spiral specimens showed reinforcement in load capacity compared to hoop specimens. High-reinforcement ratio specimens (3.55%) failed explosively but were somewhat ductile due to concrete crushing accompanied by rupturing of GFRP bars, and these specimens' exhibited indications of stress evolution in the specimen during most of the test period, represented by the rupturing sounds of longitudinal and transverse GFRP bars. The general nature of failure in the GFRP-RPC spiral specimens was more efficient in preserving the concrete core despite the crushing of the surrounding concrete upon failure. In contrast, the failure of low-reinforcement ratio specimens (1.77 %) was brittle because it was predominantly controlled by the failure of longitudinal GFRP bars, giving only minor indications before catastrophic failure, characterized by crushing of the concrete cover and rupturing of most longitudinal GFRP bars. High-reinforcement ratio specimens exhibited ductile and better confinement efficiency than low-reinforcement ratio specimens. It is worth noting that high reinforcement ratios contributed to reducing the buckling of longitudinal GFRP bars.

6.2. Influence of transverse reinforcement ratio

The low-reinforcement ratio specimens (1.24 %) failed in a brittle and explosive manner compared to the higher reinforcement ratio specimens (1.65 % and 2.48 %). Increasing the transverse reinforcement ratio from 1.24 to 1.65 % in the GFRP-RPC hoop specimens contributed to an increase in load capacity ranging from approximately 3.7 to 13.19 %. Increasing the transverse reinforcement ratio from 1.24 to 2.48 % in the GFRP-RPC hoop specimens contributed to an increase in load capacity ranging from approximately 9.91 to 19.1 %. Additionally, increasing the transverse reinforcement ratio from 1.24 to 1.65 % in the GFRP-RPC spiral specimens contributed to an increase in load capacity ranging from approximately 1 to 8.88 %. Increasing the transverse reinforcement ratio from 1.24 to 2.48 % in the GFRP-RPC spiral specimens contributed to an increase in load capacity ranging from approximately 5.13 to 15.05 %. The influence of the transverse reinforcement ratio on the ultimate load for hoop and spiral specimens is illustrated in Fig. 43 and Fig. 44, respectively.

From the previous results, it is evident that an increase in the transverse reinforcement ratio leads to a significant improvement in load capacity. Although the ultimate loads of spiral specimens surpass those of hoop specimens, the extent of improvement in the ultimate loads for hoop specimens exceeds the improvement for spiral specimens. This can be attributed to the fact that specimens with a reinforcement ratio of 2.48% enhance the bond between the reinforcement and concrete. Additionally, the higher ratio works to increase the tensile strength of the reinforcement, allowing the specimen to stretch further before reaching failure, thereby increasing its ability to carry additional loads. Moreover, the distribution of forces is related to this, as additional transverse reinforcement helps distribute the forces more effectively, reducing their concentration at specific points, increasing load distribution, and making the specimen more stable. The superiority of spiral specimens can be explained by the fact that spirals have an increasing bending resistance due to their design, which makes them a cohesive unit, preventing the concentration of forces at specific points, and thus avoiding weak areas in the transverse reinforcement. Additionally, this can be attributed to the increase in effective length within the spiral specimens because it works to direct the spirals in a twisted manner around the transverse bars, which contributes to an increase in load capacity. The general nature of failure in the high transverse reinforcement ratio (2.48%) GFRP-RPC spiral specimens was more efficient in maintaining the integrity of the concrete core despite the crushing of the surrounding concrete upon failure compared to the hoop specimens. In contrast, failure in the low transverse reinforcement ratio (1.24%) specimens was brittle and only exhibited slight indications before catastrophic failure, characterized by the crushing of the concrete cover and the rupturing of most of the transverse GFRP bars, even in cases with a high longitudinal reinforcement ratio. The high reinforcement ratio specimens showed better ductility and confinement efficiency compared to the low reinforcement ratio specimens, which will be discussed in subsequent sections. It is worth noting that high transverse reinforcement ratios somewhat contributed to reducing the twisting of longitudinal GFRP bars.

6.3. Influence of Transverse Reinforcement Configuration (Hoops vs. Spirals)

GFRP-RPC specimens confined with GFRP spirals showed better ductility and confinement efficiency as opposed to GFRP-RPC specimens confined with GFRP hoops. This is attributed to the effective confinement of the concrete core, which resulted in uniform pressure distribution along the perimeter and along the specimen height. Furthermore, the difference becomes evident after crushing the concrete cover of well-confined specimens (G8-S40 and G8-H40). Additionally, it was observed that specimens reinforced with GFRP spirals showed a greater load capacity compared to those reinforced with GFRP hoops. The load capacities for specimens G4-S40, G6-S40, and G8-S40 were 1058, 1356.2, and 1653.2 kN, respectively, representing an increase of 9.95, 13.98, and 17.27% compared to the load capacities of specimens G4-H40, G6-H40, and G8-H40, which are equal to 962.2, 1189.8, and 1409.7 kN, respectively. The load capacities for specimens G4-S60, G6-S60, and G8-S60 were 1025, 1283.5, and 1509 kN, respectively, representing an increase of 12.57, 13.5, and 13.6% compared to the load capacities of specimens G4-H60, G6-H60, and G8-H60, which are equal to 910.5, 1130.8, and 1328.3 kN. The load capacities for specimens G4-S80, G6-S80, and G8-S80 were 1006.3, 1178.8, and 1494.2 kN, respectively, representing an enhancement of 14.95, 18, and 16.65% as opposed to the load capacities of specimens G4-H80, G6-H80, and G8-H80, which are equal to 875.4, 999, and 1280.9 kN. The overall behavior of the hoop specimens was brittle upon failure, except for specimens with high reinforcement ratios, which exhibited ductile behavior.

6.4. Influence of Type of Longitudinal Reinforcement (GFRP, Steel, and Hybrid)

The behavior of specimens G6-H60 (fully GFRP-reinforced), S6-H60 (fully steel-reinforced), and H6-H60 (hybrid-reinforced) were analyzed and compared to evaluate the influence of the longitudinal reinforcement type on the behavior of specimen under concentric loading. Each specimen was reinforced with six bars, yielding an identical longitudinal reinforcement ratio (ρ_l) of 2.66%. The Steel-RPC and Hybrid-RPC specimens showed an improvement in load capacity of 19.45 % and 14.61 %, respectively compared with the G6-H60 specimen. The post-peak load loss rate was lower in the Steel-RPC specimen, followed by the Hybrid-RPC specimen then the GFRP-RPC specimen. This can be attributed to the high compressive capacity for the longitudinal steel reinforcement that was used in the Steel-RPC and Hybrid-RPC specimens.

7. Design equations of GFRP-RPC columns

The axial load capacity of GFRP-RC columns is estimated using eleven equations. The description details of all analytical equations with their formulations are shown in Table 8. For better understanding, the analytical equations are assigned different model identities, represented in ACI 440-22 [10], CSA S807-19 [8], Hasan et al. [49], AS–3600 [50], Hadhood et al. [51], Maranan et al. [36], Hadi et al. [52], Mohamed et al. [2], Afifi et al. [53], Tobbi et al. [54], and CAN/CSA S806-12 [7].

Table 8. Details of analytical equations.

No.	The study	Equation	Description
1	ACI 440-22 [10]	$P_o = \alpha_1 f'_c A_g$	$\alpha_1 = 0.85$
2	CSA S807-19 [8]	$P_o = \alpha_1 f'_c (A_g - A_f) + f_{FRP} A_f$	$\alpha_1 = 0.85;\ f_{FRP} = 0.002E_f$
3	Hasan et al. [49]	$P_o = \alpha_1 f'_c (A_g - A_f) + \varepsilon_{co} E_f A_f$	$\alpha_1 = 0.85;\ \varepsilon_{co} = 0.0005(f'_c)^{0.4}$
4	AS–3600 [50]	$P_o = \alpha_1 f'_c (A_g - A_f) + f_{FRP} A_f$	$\alpha_1 = 0.85;\ f_{FRP} = 0.0025E_f$
5	Hadhood et al. [51]	$P_o = \alpha_1 f'_c (A_g - A_f) + f_{FRP} A_f$	$\alpha_1 = 0.85 - 0.0015f'_c$ $f_{FRP} = 0.0035E_f$
6	Maranan et al. [36]	$P_o = \alpha_1 f'_c (A_g - A_f) + f_{FRP} A_f$	$\alpha_1 = 0.9;\ f_{FRP} = 0.002E_f$
7	Hadi et al. [52]	$P_o = \alpha_1 f'_c (A_g - A_f) + \varepsilon_f E_f A_f$	$\alpha_1 = 0.85;\ \varepsilon_f = 0.003$
8	Mohamed et al. [2]	$P_o = \alpha_1 f'_c (A_g - A_f) + \varepsilon_f E_f A_f$	$\alpha_1 = 0.85;\ \varepsilon_f = 0.002$
9	Afifi et al. [53]	$P_o = \alpha_1 f'_c (A_g - A_f) + \alpha_f f_{fu} A_f$	$\alpha_1 = 0.85;\ \alpha_f = 0.25$
10	Tobbi et al. [54]	$P_o = \alpha_1 f'_c (A_g - A_f) + \alpha_f f_{fu} A_f$	$\alpha_1 = 0.85;\ \alpha_f = 0.35$
11	CAN/CSA S806-12 [7]	$P_o = \alpha_1 f'_c (A_g - A_f)$	$\alpha_1 = 0.85 - 0.0015f'_c \geq 0.67$

* ε_{co} in Hasan et al., equation was calculated using an equation that gave good agreement with the measured experimental value proposed by Leggeron and Poulter [55].

The theoretical load was calculated for each equation, and then the experimental load (resulting from actual testing) was divided by the theoretical load (calculated from the above equations). From this ratio, three of the most important statistical parameters were extracted: average, standard deviation (SD) coefficient, and coefficient of variation (COV). These parameters provide clear indicators of the consistency and reliability of a specific equation compared to other equations. As is known, an equation yielding an average close to one provides better predictions than other equations. Furthermore, an equation yielding a high standard deviation indicates lower reliability (dispersed values). Lastly, dispersion decreases and accuracy increases when the coefficient of variation of an equation is lower than that of other equations. The ratios of experimental and theoretical load capacities of GFRP-reinforced circular concrete columns are illustrated in Table 9. The results indicate that equations that neglected the contribution of GFRP bars in calculations of the load capacity (ACI 440-22 and CSA S806-12) yielded high COV values (18.76 for ACI 440-22 and 19.37 for CSA S806-12). Similarly, high SD values were observed (0.177 for ACI 440-22 and 0.22 for CSA S806-12). The resulting average was 0.94 for ACI 440-22 and 1.14 for CSA S806-12. Furthermore, equations utilizing the tensile strength of the GFRP bars (Tobbi and Afifi) in the load capacity calculations demonstrated lower COV and SD values compared to equations depending on the axial strain or modulus of elasticity of longitudinal GFRP bars (CSA S807-19, AS–3600, Hadhood, Maranan, Hadi, and Mohamed), even compared to those considering axial strain of GFRP bars equal to concrete strain at the peak stress (Hasan). Generally, the optimal average was found in Hadhood equal to 1.06, while

the remaining values ranged from 0.89 to 0.94 for ACI 440-22, CSA S807-19, Hasan, AS–3600, Maranan, Hadi, and Mohamed. However, the averages were lower for Afifi, and Tobbi equal to 0.88. It has been observed that the CAN/CSA S806-12 [7] average was conservative with a safety factor of 14%. For design purposes, it is known that designers prefer equations with a reasonably conservative safety margin over those that overestimate or provide exact theoretical results to ensure an adequate safety margin in case of design flaws. Therefore, the application of equations by Hadhood et al. [51] and CAN/CSA S806-12 [7], which have a reasonable safety factor equal to 6 and 14%, respectively, are recommended, while the application of other equations may slightly increase the construction cost. However, this does not imply that equations should not be considered. Finally, the Hadhood equation is somewhat more widely accepted due to its possession of a reasonable safety factor compared to all other equations. It also has the second-best COV at 17.84, following the Afifi, and Tobbi equations with 17.11. This is despite having the second-highest SD with a value of 0.19. In conclusion, equations that incorporate the tensile strength of the GFRP bars in calculating the axial load capacity of reinforced concrete columns with GFRP bars provide relatively acceptable safety and greater reliability compared to others, with less dispersion.

Table 9. Ratios of the experimental to theoretical axial load capacities of GFRP bar-reinforced circular concrete columns.

No.	Specimens	$P_{exp.}/P_o$ Equation number										
		1	**2**	**3**	**4**	**5**	**6**	**7**	**8**	**9**	**10**	**11**
1	G4-H40	0.75	0.75	0.74	0.75	0.86	0.71	0.74	0.75	0.72	0.72	0.90
2	G6-H40	0.93	0.93	0.91	0.92	1.05	0.88	0.91	0.93	0.87	0.87	1.12
3	G8-H40	1.10	1.09	1.07	1.08	1.23	1.04	1.07	1.09	1.01	1.01	1.34
4	G4-H60	0.71	0.71	0.70	0.71	0.82	0.67	0.70	0.71	0.68	0.68	0.85
5	G6-H60	0.89	0.88	0.87	0.87	1.00	0.83	0.87	0.88	0.83	0.83	1.07
6	G8-H60	1.04	1.03	1.01	1.02	1.16	0.98	1.01	1.03	0.95	0.95	1.26
7	G4-H80	0.69	0.68	0.68	0.68	0.79	0.65	0.68	0.68	0.65	0.65	0.82
8	G6-H80	0.78	0.78	0.77	0.77	0.89	0.74	0.77	0.78	0.73	0.73	0.94
9	G8-H80	1.00	0.99	0.98	0.98	1.12	0.94	0.97	0.99	0.91	0.91	1.22
10	G4-S40	0.83	0.83	0.82	0.82	0.95	0.78	0.82	0.83	0.79	0.79	0.99
11	G6-S40	1.06	1.06	1.04	1.05	1.20	1.00	1.04	1.06	0.99	0.99	1.28
12	G8-S40	1.29	1.28	1.26	1.27	1.45	1.21	1.26	1.28	1.18	1.18	1.57
13	G4-S60	0.80	0.80	0.79	0.80	0.92	0.76	0.79	0.80	0.77	0.77	0.96
14	G6-S60	1.01	1.00	0.98	0.99	1.14	0.94	0.98	1.00	0.94	0.94	1.21
15	G8-S60	1.18	1.17	1.15	1.16	1.32	1.11	1.15	1.17	1.08	1.08	1.44
16	G4-S80	0.79	0.78	0.78	0.78	0.90	0.74	0.78	0.78	0.75	0.75	0.94
17	G6-S80	0.92	0.92	0.90	0.91	1.05	0.87	0.90	0.92	0.86	0.86	1.11
18	G8-S80	1.17	1.16	1.14	1.15	1.31	1.10	1.14	1.16	1.07	1.07	1.42
Avg.		0.94	0.94	0.92	0.93	1.06	0.89	0.92	0.94	0.88	0.88	1.14
SD		0.177	0.174	0.168	0.171	0.190	0.165	0.168	0.174	0.150	0.150	0.220
COV (%)		18.76	18.60	18.25	18.41	17.84	18.64	18.23	18.60	17.11	17.11	19.37

8. Conclusions

Based on the results of the experimental tests, the following conclusions can be drawn:

- The GFRP-RPC columns behaved similarly to the Steel-RPC, and Hybrid-RPC columns and showed linear load-strain behavior in the ascending part up to 85% of their peak loads. Moreover, the failure modes of the GFRP-RPC columns were rupture or buckling of longitudinal GFRP bars and rupture of GFRP hoops or spirals in the upper half region or center.
- The failure mode of GFRP-RPC columns can be controlled by reducing the spacing between hoops or spirals. The results indicate that GFRP-RPC columns with close spacing (40 mm) failed in a somewhat ductile manner. Conversely, columns with larger spacing (60 and 80 mm) failed in a brittle and explosive manner.
- Most GFRP-RPC columns failed due to GFRP bar rupture followed by concrete crushing, while Steel-RPC column specimens failed due to steel buckling followed by concrete crushing. The failure of the Hybrid-RPC column specimen involved a combination of GFRP bar rupture and steel bar buckling, followed by concrete crushing. Interestingly, some columns showed spalling of concrete before crushing of concrete.
- Increasing the longitudinal reinforcement ratio significantly enhances load capacity. In the GFRP-RPC hoops specimens, the increase in longitudinal reinforcement ratio from 1.77 to 3.55% increases the load capacity by 46%, while for spirals specimens the increase ratio was from 47.22 to 56.25%.
- Increasing the transverse reinforcement ratio significantly enhances load capacity. For instance, an increase in transverse reinforcement ratio from 1.24 to 2.48% in the GFRP-RPC specimens contributed to an increase in load capacity ranging from approximately 5.13 to 19.1 %. Furthermore, when increasing the transverse reinforcement ratio, hoop specimens showed a high improvement in load capacity compared to spiral specimens. For instance, an increase in transverse reinforcement ratio from 1.24 to 2.48% in the GFRP-RPC hoop specimens contributed to an increase in load capacity ranging from approximately 9.91 to 19.1% while in the GFRP-RPC spirals specimens contributed to an increase in load capacity ranging from approximately 5.13 to 15.05 %.
- Increasing the longitudinal reinforcement ratio from 1.77 to 2.66% and

from 1.77 to 3.55%, the axial displacement decreased by 58.12% and 67.59%, respectively, and when the transverse reinforcement ratio increased from 1.24 to 1.65% and from 1.24 to 2.48%, the axial displacement was reduced by 17.01 and 45.96%, respectively.

- Experimental results signified that the use of GFRP spirals as transverse reinforcement effectively confined the concrete core even after failure.
- The load capacity of the GFRP-RPC column was, on average, 16.3% and 12.8% lower than their counterparts, Steel-RPC and Hybrid-RPC.
- As the ratio of longitudinal reinforcement increased, the average load capacity of longitudinal GFRP bars in GFRP-RPC columns also increased. The contribution of GFRP bars ranged from 1.6% to 4.6% of the ultimate load capacity for GFRP-RPC columns. These lower values can be attributed to the use of RPC, which reduced the contribution of reinforcement and increased the contribution of concrete.
- The ductility of GFRP-RPC columns confined with GFRP spirals was higher than that of GFRP-RPC columns confined with GFRP hoops with an average ductility index of 2.1 for all spiral specimens, while the average ductility index for all hoop specimens was 1.99. The columns with a smaller spacing of hoops/spirals presented higher ductility than the columns with a larger spacing. Furthermore, it was found that an increase in the longitudinal reinforcement ratio also contributed to improving the ductility index.
- The results of the assessment of available code equations and researchers have shown that the Hadhood equation provides reasonable predictions for estimating the ultimate load capacity of circular concrete columns reinforced with GFRP bars. Furthermore, equations that incorporate the tensile strength of the GFRP bars in calculating the axial load capacity of reinforced concrete columns with GFRP bars provide relatively acceptable safety and greater reliability with less dispersion compared to other equations that depend on the axial strain or modulus of elasticity of longitudinal GFRP bars, even compared to those considering axial strain of GFRP bars equal to concrete strain at the peak stress.
- The evaluation of modern design equations revealed that the CSA S807-19 equation (which includes GFRP bar contribution) and the ACI.440-22 equation (which ignores GFRP bar contribution) were nearly symmetrical and exhibited good predictive capacity. This indicates that neglecting the contribution of GFRP bars when calculating the ultimate axial capacity of columns would not significantly affect their nominal load capacity.
- Based on the study's results, it can be concluded that GFRP reinforcement is a suitable alternative to steel, especially in columns exposed to corrosion, the specimens with a reinforcement ratio of 1.77% showed brittle failure and failure was sudden without warning. Therefore, we suggest reconsidering what was stated in ACI 440-22 and be the minimum reinforcement ratio is not less than 2.5%.

Authors' contribution

All authors contributed equally to the preparation of this article.

Declaration of competing interest

The authors declare no conflicts of interest.

Funding source

This study didn't receive any specific funds.

Data availability

The data that support the findings of this study are available from the corresponding author upon reasonable request.

Acknowledgments

The authors would like to express their thankfulness to the Civil Engineering Department, College of Engineering, Mustansiriyah University in Baghdad, Iraq, and the editorial team of the Qadisiyah Journal for Engineering Sciences (QJES), for their support of scientific research efforts.

REFERENCES

[1] Z.S. Othman, A.H. Mohammad, Behaviour of eccentric concrete columns reinforced with carbon fibre-reinforced polymer bars, Advances in civil engineering, 2019(1769212) (2019) 13. https://doi.org/10.1155/2019/1769212

[2] H.M. Mohamed, M.Z. Afifi, B. Benmokrane, Performance evaluation of concrete columns reinforced longitudinally with FRP bars and confined with FRP hoops and spirals under axial load, Journal of Bridge Engineering, 19(7) (2014) 04014020. https://doi.org/10.1061/(ASCE)BE.1943-5592.0000590

[3] ACI 440.1R-15, Guide for the Design and Construction of Structural Concrete Reinforced with FRP Bars, American Concrete Institute (ACI), Committee ACI, Farmington Hills, USA, 2015.

[4] H.M. Mohamed, B. Benmokrane, Design and performance of reinforced concrete water chlorination tank totally reinforced with GFRP bars: Case study, Journal of Composites for Construction, 18(1) (2014) 05013001. https://doi.org/10.1061/(ASCE)CC.1943-5614.0000429

[5] R.Z. Hamed, H.F. Hassan, Structural Behavior of GFRP-RC Slender Columns Under Various Eccentricity Loading Conditions, Civil And Environmental Engineering Reports, 19(1) (2023) 1-16. https://doi.org/10.2478/cee-2023-0001

[6] H.F. Hassan, R.Z. Hamed, Fiber RC-FRP columns under various eccentricity loading conditions: State of art review, AIP Conference Proceedings: AIP Publishing, 2787(1) (2023, July) 080035. https://doi.org/10.1063/5.0148887

[7] CAN/CSA S806-12, Design and construction of building components with fiber reinforced polymers, Canadian Standard Association (CSA), Mississauga, Ontario, Canada, 2012.

[8] CSA S807-19, Specification for Fibre-Reinforced Polymers, Canadian Standard Association (CSA), Toronto, Ontario, Canada, 2019.

[9] ACI: 440.1R-06, Guide for the Design and Construction of Structural Concrete Reinforced with FRP Bars, American Concrete Institute (ACI), Farmington Hills, MI, USA, 2006.

[10] ACI Code 440.11-22, Building Code Requirements for Structural Concrete Reinforced with Glass Fiber-Reinforced Polymer (GFRP) Bars: Code and Commentary, American Concrete Institute (ACI), ACI Committee 440, Farmington Hills, MI, USA, 2022.

[11] P. Richard, M. Cheyrezy, Composition of reactive powder concretes, Cement and concrete research, 25(7) (1995) 1501-1511. https://doi.org/10.1016/0008-8846(95)00144-2

[12] H. Li, F. Wu, L. Bu, Y. Liu, J. Yao, Study on the compression performance of steel reactive powder concrete columns, Advances in Structural Engineering, 23(10) (2020) 2018-2029. https://doi.org/10.1177/1369433220903986

[13] A.H. Mohammed, L.A.G. Yassin, M.M. Hamid, Experimental investigation on the ultimate capacity of rectangular reinforced hybrid concrete columns under axial load, GEOMATE Journal, 23(95) (2022) 112-118. https://doi.org/10.21660/2022.95.3210

[14] L. Zhang, M. Zhang, K. Wang, J. Shi, W. Chen, K. Yan, Axial compressive behavior of steel-reinforced reactive powder concrete short columns, Structures, 46(2022) 433-444. https://doi.org/10.1016/j.istruc.2022.10.073

[15] M.N.S. Hadi, H.A. Hasan, M.N. Sheikh, Experimental Investigation of Circular High-Strength Concrete Columns Reinforced with Glass Fiber-Reinforced Polymer Bars and Helices under Different Loading Conditions, Journal of Composites for Construction, 21(4) (2017) 04017005. https://doi.org/10.1061/(ASCE)CC.1943-5614.0000784

[16] N.P. Duy, V.N. Anh, N. Minh, T. Anh, P.A. Eduardovich, Load-Carrying Capacity of Short Concrete Columns Reinforced with Glass Fiber Reinforced Polymer Bars Under Concentric Axial Load, International Journal of Engineering and Advanced Technology, 9(2) (2019) 1712-1719. https://doi.org/10.35940/ijeat.b2372.129219

[17] S. El Gamal, O. Alshareedah, Experimental Study on the Performance of Circular Concrete Columns Reinforced with GFRP under Axial Load, International Conference on Civil Infrastructure and Construction (CIC 2020), (2020, February) 877-885. https://doi.org/10.29117/cic.2020.0115

[18] M. Elchalakani, T. Aly, W. Nawaz, Behavior of Circular concrete columns reinforced with GFRP bars and spirals under axial and eccentric loading, Concrete Institute of Australia's 30th National Conference 2021, Australian Concrete Institute, (2021, September) 1-8. http://www.ciaconference.com.au/concrete2021/pdf/full-paper_25.pdf

[19] M.G. Gouda, H.M. Mohamed, A.C. Manalo, B. Benmokrane, Behavior of Hollow Glass Fiber-Reinforced Polymer-Reinforced Concrete Columns under Axial Load: Experimental and Theoretical Investigation, ACI Structural Journal, 119(6) (2022) 289-302. https://doi.org/10.14359/51736117

[20] H.F. Hassan, Punching Shear Behavior of Normal and Modified Reactive Powder Concretes Slabs, PhD dissertation, Civil Engineering Department, Mustansiriyah University, Baghdad, Iraq, 2012.

[21] ASTM C109/C109M-21, Standard Test Method for Compressive Strength of Hydraulic Cement Mortars (Using 2-in. or [50 mm] Cube Specimens), American Society for Testing and Materials (ASTM), Committee C-1 on Cement, ASTM International, West Conshohocken, PA, USA, 2021. https://doi.org/10.1520/C0109_C0109M-21

[22] ASTM C1437-20, Standard Test Method for Flow of Hydraulic Cement Mortar, American Society for Testing and Materials (ASTM), Committee C-1 on Cement, ASTM International, West Conshohocken, PA, USA, 2020. https://doi.org/10.1520/C1437-20

[23] P. Richard, M.H. Cheyrezy, Reactive powder concretes with high ductility and 200-800 MPa compressive strength, Special Publication in ACI Spring Convention, 144(1994) 507-518. https://doi.org/10.14359/4536

[24] R. Messer, K., Fahem, A., T. Guthai, A., P. Singh, R. (2022). 'The experimental methods and elastic properties of shale bedding planes materials state-of-the-art review', *Al-Qadisiyah Journal for Engineering Sciences*, 15(2), pp. 126-130. doi: 10.30772/qjes.v15i2.823

[25] Fahem, A.F., Thumbalam Guthai, A. & Singh, R.P. Full-Field Strain Measurement Integrated with Two Dimension Regression Analysis to Evaluate the Bi-Modulus Elastic Properties of Isotropic and Transversely Isotropic Materials. Exp Mech 64, 53–71 (2024). https://doi.org/10.1007/s11340-023-01007-z

[26] ASTM C39/C39M-21, Standard Test Method for Compressive Strength of Cylindrical Concrete Specimens, American Society for Testing and Materials (ASTM), ASTM International, West Conshohocken, PA, USA, 2021. https://doi.org/10.1520/C0039_C0039M-21

[27] ASTM C496/C496M-17, Standard Test Method for Splitting Tensile Strength of Cylindrical Concrete Specimens, American Society for Testing and Materials (ASTM), ASTM International, West Conshohocken, PA, USA, 2017. https://doi.org/10.1520/C0496_C0496M-17

[28] Nanjing Fenghui Composite Co. Ltd._China: producer of composite reinforcing elements for design and construction. China.

[29] ASTM D7205/D7205M-21, Standard Test Method for Tensile Properties of Fiber Reinforced Polymer Matrix Composite Bars, American Society for Testing and Materials (ASTM), ASTM International, West Conshohocken, PA, USA, 2021. https://doi.org/10.1520/D7205_D7205M-21

[30] ASTM A615/A615M-22, Standard Specification for Deformed and Plain Carbon-Steel Bars for Concrete Reinforcement, American Society for Testing and Materials (ASTM), ASTM International, West Conshohocken, PA, USA, 2022. https://doi.org/10.1520/A0615_A0615M-22

[31] M.Z. Afifi, H.M. Mohamed, B. Benmokrane, Theoretical stress–strain model for circular concrete columns confined by GFRP spirals and hoops, Engineering Structures, 102(2015) 202-213. https://doi.org/10.1016/j.engstruct.2015.08.020

[32] J. Tu, K. Gao, L. He, X. Li, Experimental study on the axial compression performance of GFRP-reinforced concrete square columns, Advances in Structural Engineering, 22(7) (2019) 1554-1565. https://doi.org/10.1177/1369433218817988

[33] A. Raza, Q.U.Z Khan, Experimental and theoretical study of GFRP hoops and spirals in hybrid fiber reinforced concrete short columns, Materials and Structures, 53(139) (2020) 1-14. https://doi.org/10.1617/s11527-020-01575-9

[34] A. Elhamaymy, H.M. Mohamed, B. Benmokrane, Durability assessment and behavior under axial load of circular GFRP-RC piles conditioned in severe simulated marine environment, Engineering Structures, 249(2021) 113376. https://doi.org/10.1016/j.engstruct.2021.113376

[35] W. Prachasaree, S. Piriyakootorn, A. Sangsrijun, S. Limkatanyu, Behavior and performance of GFRP reinforced concrete columns with various types of stirrups, International Journal of Polymer Science (2015) 237231. https://doi.org/10.1155/2015/237231

[36] G.B. Maranan, A.C. Manalo, B. Benmokrane, W. Karunasena, P. Mendis, Behavior of concentrically loaded geopolymer-concrete circular columns reinforced longitudinally and transversely with GFRP bars, Engineering Structures, 117(2016) 422-436. https://doi.org/10.1016/j.engstruct.2016.03.036

[37] A. Raza, A. Ahmad, Investigation of HFRC columns reinforced with GFRP bars and spirals under concentric and eccentric loadings, Engineering Structures, 227(2021) 111461. https://doi.org/10.1016/j.engstruct.2020.111461

[38] M. Elchalakani, G. Ma, Tests of glass fibre reinforced polymer rectangular concrete columns subjected to concentric and eccentric axial loading, Engineering Structures, 151(2017) 93-104. https://doi.org/10.1016/j.engstruct.2017.08.023

[39] M. Elchalakani, M. Dong, A. Karrech, G. Li, M.S. Mohamed Ali, B. Yang, Experimental investigation of rectangular air-cured geopolymer concrete columns reinforced with GFRP bars and stirrups, Journal of Composites for Construction, 23(3) (2019) 04019011. https://doi.org/10.1061/(ASCE)CC.1943-5614.0000938

[40] M.Z. Afifi, H.M. Mohamed, B. Benmokrane, Axial Capacity of Circular Concrete Columns Reinforced with GFRP Bars and Spirals, Journal of Composites for Construction, 18(1) (2014) 04013017. https://doi.org/10.1061/(ASCE)CC.1943-5614.0000438

[41] S. El-Gamal, O. AlShareedah, Behavior of Axially Loaded Low Strength Concrete Columns Reinforced with GFRP Bars and Spirals, Engineering Structures, 216(2020) 110732. https://doi.org/10.1016/j.engstruct.2020.110732

[42] H. Karim, B. Noel-Gough, M.N. Sheikh, M.N.S. Hadi, Strength and ductility behavior of circular concrete columns reinforced with GFRP bars and helices, FRPRCS-12/APFIS-2015 - Joint Conference of the 12th International Symposium on Fiber Reinforced Polymers for Reinforced Concrete Structures (FRPRCS -12) and the 5th Asia-Pacific Conference on Fiber Reinforced Polymers in Structures (APFIS -2015), (2015, December).

[43] A. Tabatabaei, A. Eslami, H.M. Mohamed, B. Benmokrane, Compression Splices of GFRP Bars in Unconfined and Confined Concrete Columns, Journal of Composites for Construction, 23(6) (2019) 04019046. https://doi.org/10.1061/(ASCE)CC.1943-5614.0000974

[44] C.P. Pantelides, M.E. Gibbons, L.D. Reaveley, Axial Load Behavior of Concrete Columns Confined with GFRP Spirals, Journal of Composites for Construction, 17(3) (2013) 305-313. https://doi.org/10.1061/(ASCE)CC.1943-5614.0000357

[45] M. Elchalakani, M. Dong, A. Karrech, M.S. Mohamed Ali, J.S. Huo, Circular Concrete Columns and Beams Reinforced with GFRP Bars and Spirals under Axial, Eccentric, and Flexural Loading, Journal of Composites for Construction, 24(3) (2020) 04020008. https://doi.org/10.1061/(ASCE)CC.1943-5614.0001008

[46] M.N.S. Hadi, S. Ali, M.N. Sheikh, Experimental Study of GFRP-Reinforced Geopolymer Concrete Columns under Different Loading Conditions, Journal of Composites for Construction, 25(6) (2021) 04021052. https://doi.org/10.1061/(ASCE)CC.1943-5614.0001164

[47] S. Ali, Behavior of Fiber Reinforced Geopolymer Concrete Circular Columns Reinforced with GFRP Bars and GFRP Helices under Different Loading Conditions, PhD dissertation, University of Wollongong, Wollongong, New South Wales, Australia, 2021.

[48] H.A. Hasan, M.N. Sheikh, M.N.S. Hadi, Performance evaluation of high strength concrete and steel fibre high strength concrete columns reinforced with GFRP

bars and helices, Construction and Building Materials, 134(2017) 297-310. https://doi.org/10.1016/j.conbuildmat.2016.12.124

[49] H.A. Hasan, M.N. Sheikh, M.N.S. Hadi, Maximum axial load carrying capacity of Fibre Reinforced-Polymer (FRP) bar reinforced concrete columns under axial compression, Structures, 19(2019) 227-233. https://doi.org/10.1016/j.istruc.2018.12.012

[50] AS-3600, Concrete Structures, Australia Standards (AS), Sydney, Australia, 2018.

[51] A. Hadhood, H.M. Mohamed, B. Benmokrane, Strength of circular HSC columns reinforced internally with carbon-fiber-reinforced polymer bars under axial and eccentric loads, Construction and Building Materials, 141(2017) 366-378. https://doi.org/10.1016/j.conbuildmat.2017.02.117

[52] M.N.S. Hadi, H. Karim, M.N. Sheikh, Experimental Investigations on Circular Concrete Columns Reinforced with GFRP Bars and Helices under Different Loading Conditions, Journal of Composites for Construction, 20(4) (2016) 04016009. https://doi.org/10.1061/(ASCE)CC.1943-5614.0000670

[53] M.Z. Afifi, H.M. Mohamed, B. Benmokrane, Strength and axial behavior of circular concrete columns reinforced with CFRP bars and spirals, Journal of Composites for Construction, 18(2) (2014) 04013035. https://doi.org/10.1061/(ASCE)CC.1943-5614.0000430

[54] H. Tobbi, A.S. Farghaly, B. Benmokrane, Concrete Columns Reinforced Longitudinally and Transversally with Glass Fiber-Reinforced Polymer Bars, ACI Structural Journal, 109(4) (2012) 551–558. https://doi.org/10.14359/51683874

[55] F. Légeron, P. Paultre, Uniaxial confinement model for normal- and high-strength concrete columns, Journal of Structural Engineering, 129(2) (2003) 241-252. https://doi.org/10.1061/(ASCE)0733-9445(2003)129:2(241)